Palaeogeography, Palaeoclimatology, Palaeoecology 675 (2025) 113120

Contents lists available at ScienceDirect

Palaeogeography, Palaeoclimatology, Palaeoecology

journal homepage: www.elsevier.com/locate/palaeo

Cenozoic sandstone provenance in the Qaidam Basin of China, and its implications for the deformation history of the Tibetan Plateau

Xiaotian Shen [a], Xing Jian [a,*], Wei Zhang [a], Shuhuai Ye [a], Hanghai Liang [a], Yulu Zhuang [a], Ping Guan [b]

[a] State Key Laboratory of Marine Environmental Science, College of Ocean and Earth Sciences, Xiamen University, Xiamen 361102, PR China
[b] MOE Key Laboratory of Orogenic Belts and Crustal Evolution, School of Earth and Space Sciences, Peking University, Beijing 100871, PR China

ARTICLE INFO

Editor: Howard Falcon-Lang

Keywords:
Sandstone petrography
Cenozoic Qaidam Basin
Sedimentary provenance analysis
Tibetan Plateau

ABSTRACT

Provenance studies of Cenozoic clastic successions in the Qaidam Basin of China may provide insights into the deformation history of the Tibetan Plateau. However, diverse bedrock lithology in this region, which includes the Qilian Mountains, the Eastern Kunlun Range, and the Altun Range, complicates such analyses. In this study, we compile a comprehensive dataset of sandstone petrographic composition and texture, incorporating new ($n = 74$) and previously published ($n = 546$) data, which show significant spatial variations indicative of potential source terranes. For the northern and northeastern Qaidam Basin, feldspathic litharenite sandstones with abundant metamorphic lithics suggest dominant metamorphic sources in the Qilian Mountains, in contrast with the detrital zircon-based hypothesis that the Eastern Kunlun Range mostly fed the northeastern Qaidam Basin. Temporal changes in quartz/feldspar ratio and lithic contents are attributed to variable contributions from different parent-rocks within the Qilian Mountains. In contrast, sandstones from the western Qaidam Basin are lithic arkose with a few amounts of sedimentary lithics, indicating primary sources in the adjacent Altun and Eastern Kunlun ranges. Additionally, the quartz/lithics ratios are positively correlated with grain size and sorting, and the analyzed sandstones indicate increasing contents of mica and carbonate lithics over time, suggesting climate and sedimentary environment influenced sandstone petrographic composition and texture. Provenance analysis based on petrographic data suggests the Qaidam Basin formed as a rapid response to the India-Eurasia collision and further provide evidence for the synchronous deformation model of the northern Tibetan Plateau. Our findings highlight the importance of petrography analysis in sandstone provenance studies and emphasize the lithology differences of source terranes in controlling sedimentary systems.

1. Introduction

Aiming at excavating geological information (including parent-rock assemblages, exhumation history of source regions, and transport processes) from siliciclastic sediments, sedimentary provenance analysis provides valuable insights to understand tectonics and climate of basin-mountain systems and the interplay between the two (Weltje and von Eynatten, 2004). The Qaidam Basin, a large sedimentary basin located on the northeastern margin of the Tibetan Plateau (Fig. 1), contains extensive Cenozoic terrigenous clastic deposits which provide essential materials for investigating the far-field response to the India-Eurasia collision. The sedimentary provenance studies of its Cenozoic sedimentary strata offer critical constraints on the growth history of the Tibetan Plateau (Lu et al., 2022; Wang et al., 2022; Jian et al., 2023), the uplift and erosion of surrounding mountains (Rieser et al., 2005; Zhou et al., 2018; Lu et al., 2019, 2022), and regional climate evolution throughout the Cenozoic (Pullen et al., 2011; Nie et al., 2020; Fu et al., 2022).

The Cenozoic Qaidam Basin has been extensively studies using divers provenance analysis methods, including petrographic analysis (e.g., Rieser et al., 2005; Jian et al., 2013a; McRivette et al., 2019), single mineral geochronology, thermochronology and geochemistry (Bush et al., 2016; Cheng et al., 2016b; Wang et al., 2017; He et al., 2021; Jian et al., 2024; Ye et al., 2024), as well as elemental and isotopic geochemistry (Jian et al., 2013b; Bao et al., 2019; Sun et al., 2020a; Yan et al., 2024). However, these studies have yielded conflicting interpretation of sediment provenance, particularly for the northeastern Qaidam Basin (Ye et al., 2024 and references therein), with discrepancies arising

* Corresponding author.
E-mail address: xjian@xmu.edu.cn (X. Jian).

https://doi.org/10.1016/j.palaeo.2025.113120
Received 9 April 2025; Received in revised form 1 July 2025; Accepted 1 July 2025
Available online 5 July 2025

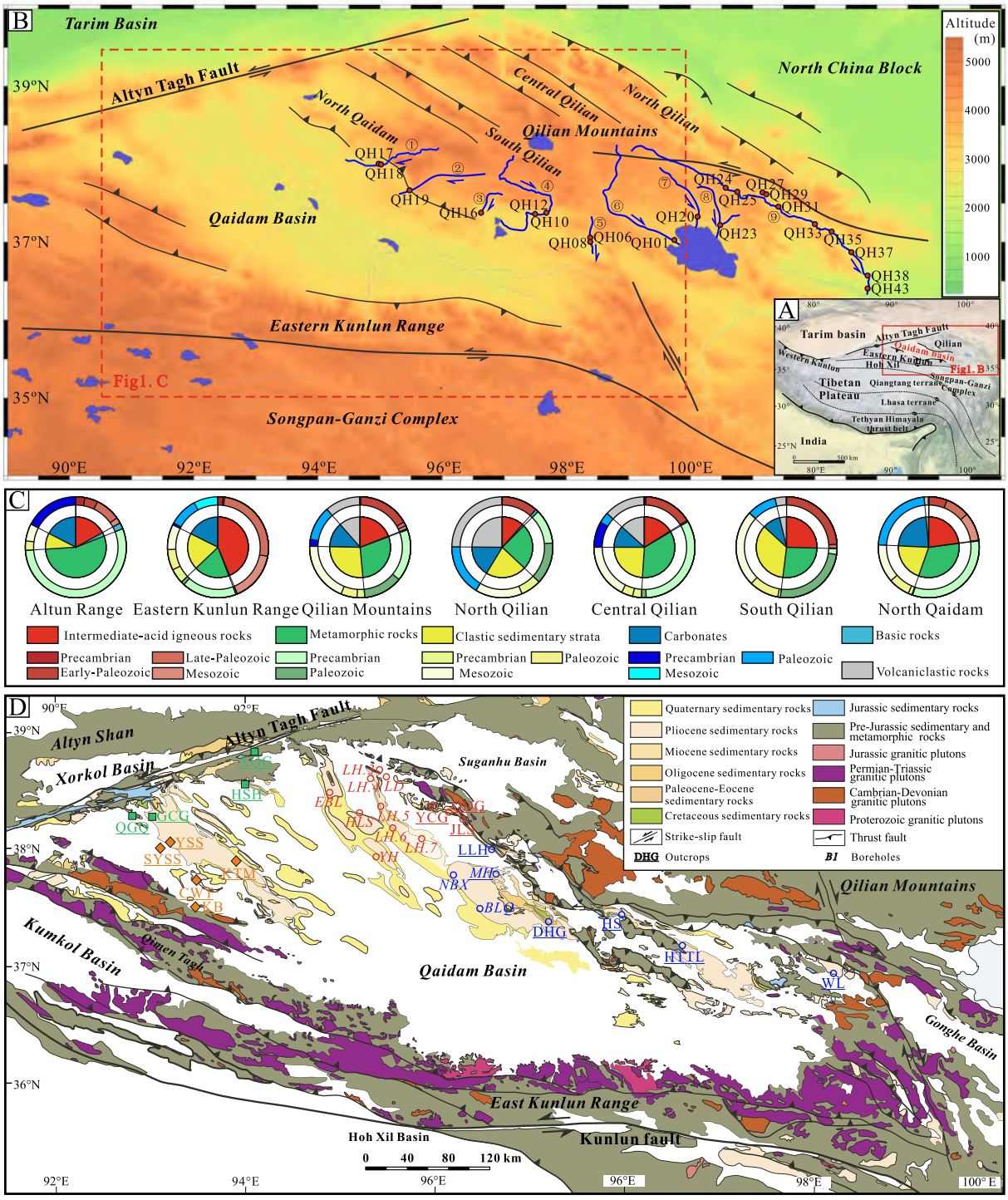

Fig. 1. Location and geological setting of the Qaidam Basin. (A) Background of the Qaidam Basin and geological units on the Tibetan Plateau. (B) Location of the Qaidam Basin in the Tibetan Plateau and surrounding orogenic belts, and locations of modern river sand samples (red dots) and involved rivers (blue lines and arrows indicating flow directions) (modified from Jian et al., 2024). Involved rivers: 1: Yuka River; 2: Tataleng River; 3: Huaitoutala River; 4: Bayinguole River; 5: Saishike River; 6: Buha River; 7: Shaliu River; 8: Haergai River; 9: Datong River. (C) Distribution of main rock types exposed in the Qilian Mountains (including four tectonic units), the Altun and Eastern Kunlun ranges. Areal percentages were calculated by point-counting method based on 1:2, 500, 000 China geological map. (D) Geological map of the Qaidam Basin and surrounding regions (modified from Lu et al., 2019). The locations of all data involved in our dataset are marked. Samples in the northern, northeastern, northwestern, and southwestern Qaidam Basin are marked by red circle, blue circle, green square, and orange diamond, respectively. Drilling wells in one region are uniformly marked by one symbol. Abbreviations in the figure: BLQ: Beilingqiu region; CWT: Changweitai section; EBL: Eboliang region; DHG: Dahonggou section; GCG: Ganchaigou section; HLS: Hulushan region; HS: Hongshan section; HSH: Hongsanhan section; HTTL: Huaitoutala section; JLS: Jielvsu section; KB: Kunbei region; KTM: Kaitemilike section; LD: Lengdong region; LH.3: No.3 Lenghu region; LH.4: No.4 Lenghu region; LH.5: No.5 Lenghu region; LH.6: No.6 Lenghu region; LH.7: No.7 Lenghu region; LLH: Lulehe section; MH: Mahai region; NBX: Nanbaxian region; QDG: Quandonggou section; QGQ: Qigequan section; SYSS: South Youshashan region; WL: Wulan Basin; XQG: Xinqugou section; YCG: Yinghcaogou section; YH: Yahu region; YSS: Youshashan region. (For interpretation of the references to colour in this figure legend, the reader is referred to the web version of this article.)

from both methodological differences and varying research objectives. Specifically, elemental and isotopic geochemical signatures from fine-grained fractions (i.e., mudstones and siltstones), dissolved fractions (e.g., sedimentary carbonates) from the sedimentary records, and detrital muscovite $^{40}Ar/^{39}Ar$ geochronology (preferentially deposited in fine-grained sediments) consistently suggest well-mixed provenance signals from multiple source terranes, due to the presence of a paleo-megalake during most of the Cenozoic depositional time (Ren et al., 2019; Liu et al., 2022, 2023; Wang et al., 2023a; Ye et al., 2024). In contrast, coarse-grained deposits predominantly reflect proximal sourcing from adjacent orogenic belts (Rieser et al., 2005; Jian et al., 2013a). For instance, sandstone petrography from the western Qaidam Basin indicate that primary derivation from the Altun Range and Qimantagh region, with minor temporal variation (Rieser et al., 2005). Detrital zircon U-Pb age distributions also show prominent peaks at 400–480 Ma and 220–280 Ma, which are consistent with the signatures of the neighboring Altun and Eastern Kunlun ranges (Bush et al., 2016; Zhu et al., 2017; Jian et al., 2024 and references therein). The current controversies are mainly about the provenance of the northern and northeastern Qaidam Basin. One proposition emphasizes the Qilian Mountains as the dominant source for the northeastern basin, based on paleocurrent orientations, sandstone petrography, heavy mineral assemblages and single mineral geochemical data (Rieser et al., 2006a, 2006b; Jian et al., 2013a; Zhu et al., 2017; Fu et al., 2022). Detrital zircon U-Pb geochronological results of samples from the northern and northeastern basin reveal a dominance of early Paleozoic ages, with subordinate Paleoproterozoic, Neoproterozoic, and Permian–Triassic ages (Jian et al., 2024 and references therein). The diagnostic 270–240 Ma zircon ages were interpreted as evidence of contributions from the south Qilian Mountains and the crystalline basement of the Qaidam Basin (Jian et al., 2024). This is further supported by prominent Permian–Triassic zircon age populations found in modern river sands sourced from the Qilian Mountains (Cheng et al., 2017; Song et al., 2019; Zhang et al., 2021; Jian et al., 2024). An alternative interpretation, mainly based on detrital zircon U-Pb geochronology, contends significant sediment supply from the distal Eastern Kunlun Range to the northern Qaidam Basin during the Paleogene, due to the prevalence of Permian–Triassic granitic rocks in the Eastern Kunlun Range (Bush et al., 2016; Wang et al., 2017, 2022).

The key controversy lies in interpretating the dominant Permian–-Triassic ages in the detrital zircon age populations from the Cenozoic Qaidam Basin sandstones (Jian et al., 2024). Despite the effectiveness and reliability of detrital zircon in sedimentary provenance analysis, the limitations of this methodology (such as zircon fertility, recycling, and grain texture) can introduce biases in provenance interpretations (e.g., Malusà et al., 2013, 2016; Chew et al., 2020; Jian et al., 2024; Shen et al., 2024). Additionally, the abundance of detrital zircon in sands or sandstones is commonly low (<1 %) (Garzanti and Andò, 2019), meaning detrital zircon U-Pb age data may reliably trace zircon-specific sources but cannot safely represent bulk sandstone provenance In contrast, petrographic analysis focuses on the framework grains of sandstones through thin-section observations of original sandstone samples. Although the petrographic approach is traditional, it is extremely fundamental and important in sandstone provenance studies. Furthermore, metasedimentary rocks and clastic sedimentary rocks are dominant in the Qilian Mountains, whereas the Eastern Kunlun Range hosts widespread Permian–Triassic plutons with subordinate metasedimentary rocks (Fig. 1). This remarkable lithological contrast makes sandstone petrography especially effective for the Qaidam Basin provenance studies. Many studies have applied petrographic analysis to Cenozoic sandstones in the Qaidam Basin. However, most have concentrated on regional source-to-sink system based on several outcrops or boreholes, such as those in western basin (e.g., Rieser et al., 2005), in northern basin (e.g., Jian et al., 2013a; Gong et al., 2023), and in northeastern basin (e.g., Bush et al., 2016; Li et al., 2021). Basin-wide petrographic analysis of the Cenozoic Qaidam Basin remains limited. We therefore advocate for a comprehensive, basin-wide petrographic analysis to better elucidate the sediment provenance of the Cenozoic Qaidam Basin.

In this contribution, we compile a dataset of sandstone petrographic composition and quantitative textural parameters by integrating new data (n = 74, including 53 northern and northeastern Qaidam Basin sandstones and 21 modern river sands) with previously published data of Cenozoic Qaidam Basin sandstones (n = 546). Our research aims to (1) revisit sandstone provenance of the Cenozoic Qaidam Basin from a petrographic perspective and its implications for the Cenozoic deformation history of the Tibetan Plateau; (2) disentangle the factors controlling sandstone petrographic composition and texture; and (3) discuss how to define the source signals, especially in the context of deep-time sediment source-to-sink studies.

2. Geological setting

2.1. Qaidam Basin

The Qaidam Basin is a triangular-shaped intermontane basin located in the northeastern Tibetan Plateau, covering an area of approximately 120,000 km^2 (Fig. 1). Situated at an elevation of 2.7–3.0 km above sea level, it contains 3–16 km thick Mesozoic and Cenozoic sedimentary successions. The basin is bounded by the Qilian Mountains to the north, the Altun Range to the west, and the Eastern Kunlun Range to the south. The basement of Qaidam Basin consists of Precambrian–Silurian metamorphic rocks which experienced at least three tectonic episodes during the Neoproterozoic, early Paleozoic, and late Paleozoic–Mesozoic (Zhang et al., 2021). The Cenozoic Qaidam Basin developed as a large synclinorium in response to the far-field effects of the India-Eurasia collision (Tapponnier et al., 2001; Yin et al., 2008a).

2.2. Potential source regions for the Cenozoic Qaidam Basin deposits

The Qilian Mountains represent a ca. 300-km-long NW-trending fold-trust belt situated along the northeastern margin of the Tibetan Plateau (Fig. 1). Tectonically, the Qilian Mountains can be divided into four subparallel domains, from north to south including the North Qilian suture, the Central Qilian Block, the South Qilian belt, and the North Qaidam ultrahigh-pressure (UHP) metamorphic belt (Fig. 1B). The North Qilian suture comprises early Paleozoic ophiolite sequences, blueschist-facies metamorphic belts, island-arc volcanic rocks and granitic plutons, Silurian flysch formations, Devonian molasse, and Carboniferous to Triassic sedimentary sequences (Fig. 1) (Song et al., 2009, and references therein). The exposed rocks within the current North Qilian suture primarily include Ordovician and Cambrian volcanoclastic rocks (25 %), Paleozoic carbonates (16 %), Mesozoic clastic sedimentary rocks (15 %), early Paleozoic igneous rocks (12 %), and Paleozoic and Precambrian metamorphic strata (11 % and 13 %; Fig. 1C). These lithological assemblages in the North Qilian suture indicate the subduction of the North Qilian Ocean lithosphere and the subsequent continent-continent collision between the Qilian Block and the North China Craton during the early Paleozoic (Zuza et al., 2018; Zhang et al., 2021). The Central Qilian Block is dominated by Proterozoic metasedimentary rocks (33 %; from low-grade greenschist to high-grade amphibolite facies), with subordinate Neoproterozoic intrusive rocks (16 %). Mesozoic sedimentary strata (18 %), early Paleozoic volcaniclastic rocks (13 %), and Precambrian carbonates (8 %) are also widely distributed. The South Qilian belt consists of ophiolitic fragments, arc volcanic rocks, amphibolite-grade metamorphic rocks (35 %), early Paleozoic igneous rocks (24 %), Silurian flysch covered by Devonian molasse and Carboniferous to Triassic sedimentary rocks (25 %). The North Qaidam UHP belt consist of various UHP metamorphic rocks (32 %), including eclogite, orthogneiss, paragneiss, granitic gneiss, which record multiple cycles continental orogenesis from the Neoproterozoic to the Paleozoic. Notably, Paleozoic and Triassic

intermediate-acid igneous rocks (23 %) are also widely exposed in current North Qaidam belt.

The Altun Range is tectonically controlled by the ca. 1600-km-long sinistral strike-slip fault, known as the Altyn Tagh Fault, which separates the Qaidam Basin from the Tarim basin (Fig. 1). The northern part of the Altun Range shares similar lithology with the Qilian Mountains (Gehrels et al., 2003). The Altun Range currently exposed Precambrian metasedimentary rocks (55 %), Precambrian carbonates (17 %), and Precambrian, Paleozoic and Mesozoic granites (17 %), and Jurassic sedimentary rocks (5 %; Fig. 1C) (Yang et al., 2006; Mattinson et al., 2007).

The Eastern Kunlun Range is a ca. 1000-km-long latitudinal belt (Fig. 1), primarily composed of Late Permian to Triassic granitoid plutons (44 %), Neoproterozoic metamorphic basement rocks (18 %), and sedimentary rocks (37 %; Fig. 1C) (Li et al., 2013; Jian et al., 2020). This range has undergone significant tectono-magmatic events and sedimentary filling history related to the successive closure of the Proto-Tethys and Paleo-Tethys Oceans during the Cambrian–Triassic (Li et al., 2013; Wu et al., 2017).

2.3. Cenozoic stratigraphy, lithology and depositional ages of the Qaidam Basin

The stratigraphic framework of the Cenozoic Qaidam Basin comprises seven units, in ascending order including Lulehe Formation (E_{1+2}), Xia Ganchaigou Formation (E_3), Shang Ganchaigou Formation (N_1), Xia Youshashan Formation (N_2^1), Shang Youshashan Formation (N_2^2), Shizigou Formation (N_2^3), Qigequan Formation (Q_{1+2}). These Cenozoic deposits exhibit spatial and temporal variability in both sedimentary environments and lithologies (Fig. 2). The northern and northeastern regions predominantly consist of siliciclastic sedimentary rocks (Jian et al., 2013a; Cheng et al., 2021), whereas the western Qaidam Basin is characterized by carbonate rocks and mixed carbonate-siliciclastic deposits (Fig. 2) (Jian et al., 2014; Wang et al., 2023a). Collectively, these rock assemblages reflect a fluvial-lacustrine environment, including alluvial fan, braided river, deltaic and lacustrine environments. Stratigraphically, the Cenozoic succession generally displays an upward trend from coarse-grained (Lulehe Formation) to fine-grained (Xia Ganchaigou, Shang Ganchaigou, and Xia Youshashan formations) to coarse-grained sediments (Shang Youshashan, Shizigou, and Qigequan formations) in most regions (Figs. 2, 3). This pattern is primarily attributed to the development of a paleo-megalake that reached its maximum extent during the Miocene (Yin et al., 2008b; Bao et al., 2017).

The depositional age model for the Cenozoic strata within the Qaidam Basin remains highly debated (Cheng et al., 2021, and references therein). Two competing models have emerged. The traditional model, based on magnetostratigraphic and biostratigraphical data, fission-track data of detrital grains as well as lithostratigraphic correlations, assigns a Paleocene age (> 50 Ma) to the initiation of the Cenozoic basin filling (Sun et al., 2005; Yin et al., 2008b; Ji et al., 2017). A younger age model suggests a late Oligocene–early Miocene (~25–20 Ma) onset of

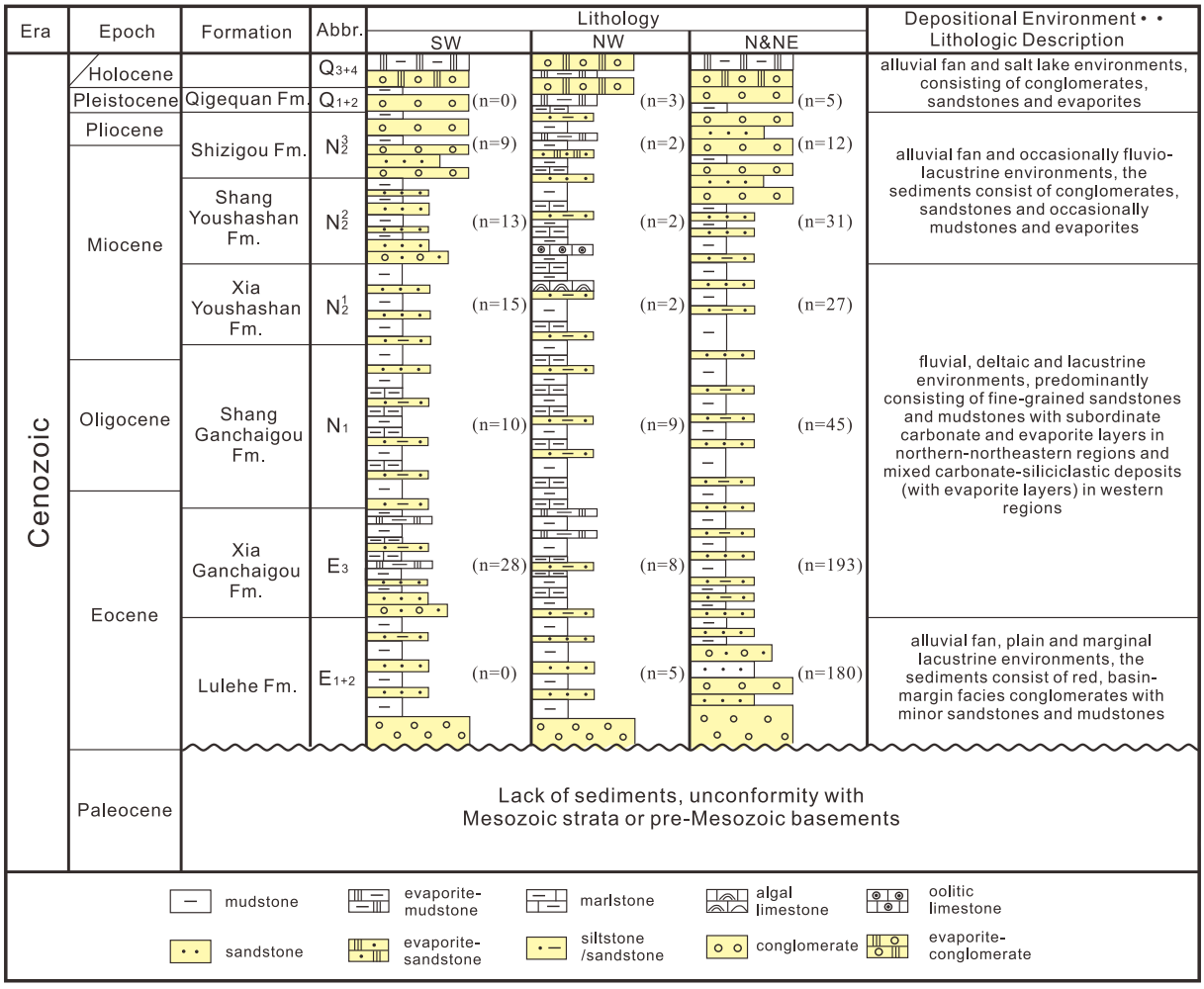

Fig. 2. Stratigraphy framework, lithology column, depositional environment and lithological description of different regions in the Cenozoic Qaidam Basin (modified from Jian et al., 2024). Numbers aside the lithological columns indicate the numbers of data within corresponding formation in the dataset.

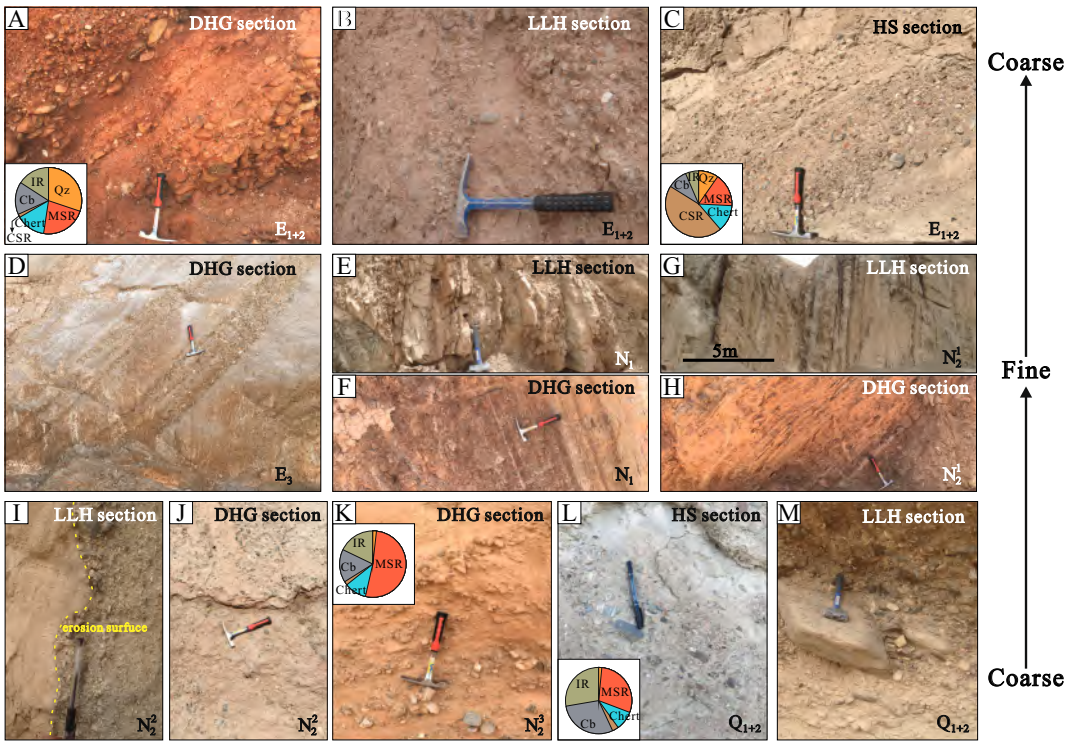

Fig. 3. Representative features of Cenozoic outcrops in the northeastern Qaidam Basin, displaying a stratigraphically coarse-fine-coarse succussion. (A) Red, thick clast-supported conglomerate bed of the DHG section (Lulehe Formation), pie chart shows the identified conglomerate clast composition which contains quartzite (Qz), meta-sedimentary rock (MSR), chert, clastic sedimentary rock (CSR), carbonate (Cb), and intermediate-acid igneous rock (IR). (B) Matrix-supported conglomerates of the LLH section (lower part of Lulehe Formation). (C) Thick clast-supported conglomerate beds of the HS section (Lulehe Formation), with dominated of sedimentary rock clasts. (D) Thick sandstones with thin bedded conglomerate of the DHG section (Xia Ganchaigou Formation). (E–H) Laminated fine-grained sedimentary rocks of the Shang Ganchaigou and Xia Youshashan formations in LLH and DHG sections. (I) Erosion surface (yellow dashed line) in the LLH section (Shang Youshashan Formation). (J) Coarse sandstone with thin interbedded conglomerate of the DHG section (Shang Youshashan Formation). (K) Matrix-supported poor-sorted conglomerate of the DHG section (Shizigou Formation), with increasing contents of meta-sedimentary clasts. (L) Thin clast-supported conglomerates of the HS section (Qigequan Formation), major components are meta-sedimentary rock, carbonate and igneous rock. (M) Poor-sorted clast-supported conglomerate of the LLH section (Qigequan Formation). Note that a coarse-fine-coarse trend is shown. (For interpretation of the references to colour in this figure legend, the reader is referred to the web version of this article.)

sedimentation based on magnetostratigraphic and biostratigraphic analyses of two sections from the northeastern Qaidam Basin (Wang et al., 2017, 2022; Nie et al., 2020). Detailed comparison of these two age models has been reviewed in previous literatures (e.g., Cheng et al., 2021; Jian et al., 2023). Recent evidence, including calcite U-Pb dating and clumped isotopes for paleosol calcareous nodules from the Lulehe Formation (Zeng et al., 2025), provides additional support for the traditional model. In this study, we prefer the traditional age model because of Eocene exhumation in the surrounding mountains (Jian et al., 2018; Li et al., 2020) and well correlation between paleoclimatic records in the Qaidam Basin with the global climatic evolution history (Guo et al., 2017; Sun et al., 2020b; Liang et al., 2021).

3. Materials and methods

3.1. Samples

For this study, a total of 53 samples from five Cenozoic outcrop sections (including Quandonggou (QDG), Jielvsu (JLS), Lulehe (LLH), Dahonggou (DHG), and Hongshan (HS) sections where sandstone petrographic results are relatively poorly reported) in the northern and northeastern Qaidam Basin were selected for petrographic analysis (Figs. 1C, 4). These samples predominantly consist of fine- to coarse-grained sandstones, with the exception of LLH-34 which is a fine-grained conglomerate. These samples encompass all seven stratigraphic units and represent sediments from alluvial, fluvial and deltaic sedimentary environments (Fig. 4; Table A2 in Supplementary material 1). For comparative analysis of detrital compositions under modern versus Cenozoic climatic conditions, we additionally collected twenty-one fine- to coarse-grained sand samples from 9 rivers draining the Qilian Mountains (Fig. 1B). The locations, host rivers, and detailed descriptions of all modern river samples are given in Table A3 in Supplementary material 1.

3.2. Field measurements

Conglomerate clast compositions were quantified in the Lulehe, Shizigou and Qigequan formations in the studied outcrop sections (Fig. 3). The measuring procedure is following Jian et al., 2023, which is counting rock types in a grid with intervals of 5-cm and a size of 50-cm by 50-cm. About 50 to 100 clasts were counted at each location. Paleocurrents orientations of the DHG and HS sections were primarily determined through pebble-cobble imbrications in conglomerate beds, cross bedding and ripple in sandstone layers.

3.3. Sandstone petrography

All Cenozoic sandstone samples were polished into standard thin sections for detrital petrography analysis. For modern river sands, fine to medium sand fractions (0.063–0.5 mm) were obtained via wet and dry sieving in order to minimize the hydrodynamic sorting effect. The 0.063–0.5 mm fractions were impregnated with araldite epoxy and cut into standard thin sections. The point-counting procedures were performed under a polarizing microscope following the Gazzi-Dickinson

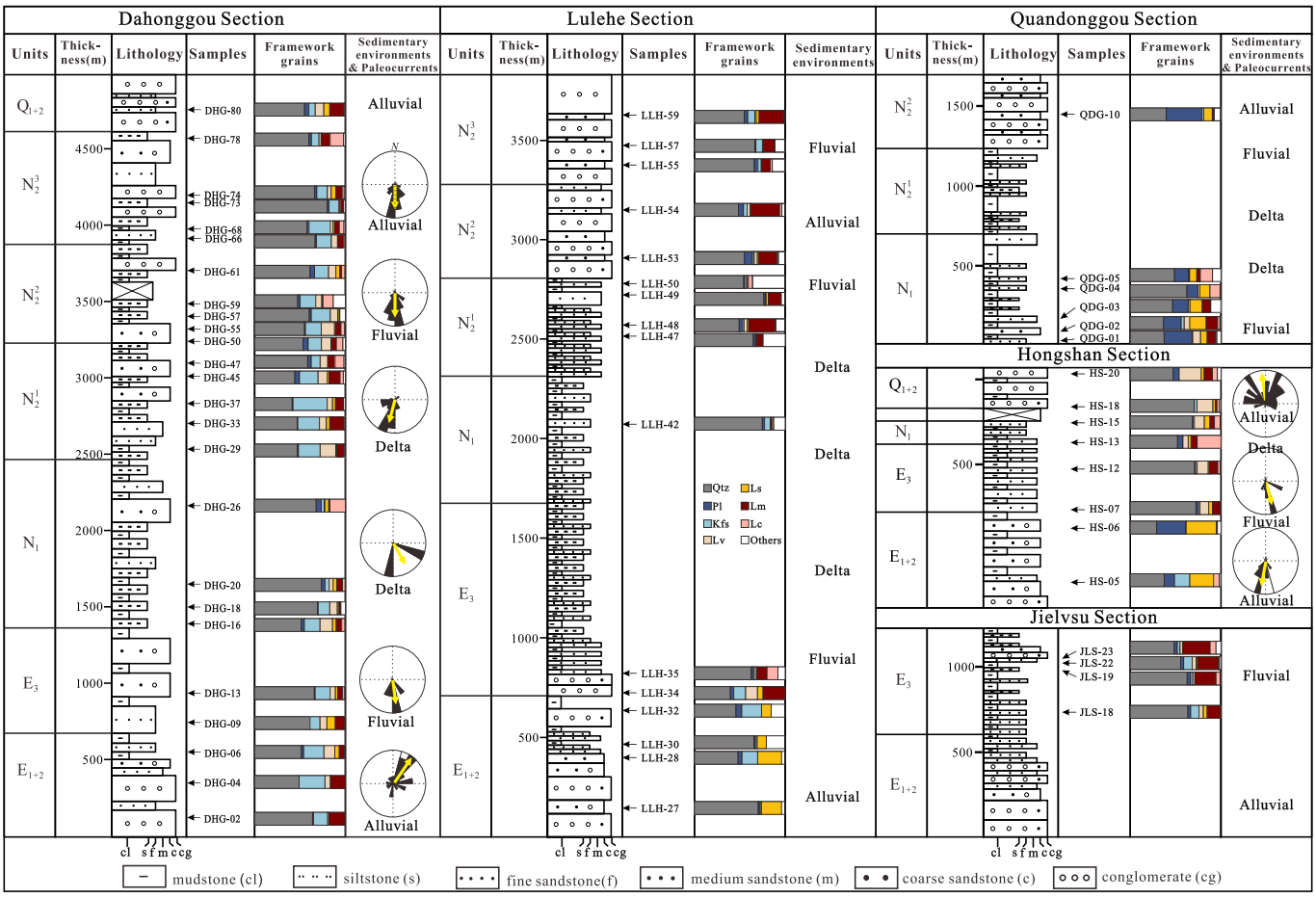

Fig. 4. Lithology, thickness, sandstone petrographic composition, sedimentary environments, and paleocurrent orientation of analyzed sections in this study. Abbreviations in the figure: Qtz: Quartz; Pl: Plagioclase; Kfs: K-feldspar; Lv: volcanic lithic fragment; Ls: sedimentary lithic fragment; Lm: metamorphic lithic fragment; Lc: carbonate lithic fragment; Others include biotite, mica, accessory minerals.

method (Dickinson and Suczek, 1979; Ingersoll et al., 1984; Dickinson, 1985), with a minimum of 400 points of each sample were counted.

In order to investigate the relationship between sedimentary environment and detrital modes, grain texture (including grain size, roundness) and sorting were quantified via image processing (detailedly described in Shen et al., 2021, 2024). All samples from the DHG and LLH sections and four samples from other three sections were selected for these measurements. Grain size was represented by equivalent spherical diameter (Garzanti et al., 2008), derived from the length (X) and width (Y) of individual grains. Length is the longest axis of grain from the two-dimensional perspective, the width is perpendicular and bisected to the length, and the third axis (Z) is assumed to be as same as the width (Lawrence et al., 2011). Then, grain size of a single grain is then computed as $(X{\cdot}Y{\cdot}Z)^{1/3}$. Roundness quantification was following the definition proposed by Wadell (1932) and processed by a Matlab-based program from Resentini et al. (2018). Grain size and roundness of more than thirty grains of each sample were quantified. Sorting was described by the relative standard deviation of the grain sizes of the measured grains within each sample.

3.4. Data compilation

Our database integrated three primary data sources: (1) original data from this study; (2) previously published articles from our research group; and (3) published articles from other research groups. All data were obtained using the Gazzi-Dickinson point-counting method and included the following components: quartz (monocrystalline quartz and polycrystalline quartz), feldspar (plagioclase, K-feldspar), lithic fragments (volcanic lithics, metamorphic lithics, clastic sedimentary lithics, carbonate lithics), and other subordinate grains (mica, heavy mineral, etc.). Most of data were derived from the literature as raw counting points or calculated percentages, while data in several articles (e.g., He et al., 2019; Chen et al., 2019) were obtained by graph data extraction. It is important to note that some literatures only provided contents of quartz, feldspar, and lithics (e.g., He et al., 2019; Chen et al., 2019; Sun et al., 2020a; Gong et al., 2023). For consistency across the dataset, all values were normalized to percentage form. Additionally, we have included a photomicrograph album in the Appendix which contains all 149 samples from our research group. Corresponding descriptions are shown in the Supplementary material 2. We hope that this collection can offer the research community an intuitive overview of the Cenozoic sandstone records from the Qaidam Basin.

4. Results

4.1. Petrographic composition of modern river sands

Modern river sands derived from the Qilian Mountains are primarily litharenite, with an average modal composition of $Q_{37}F_7L_{54}$ (Fig. 5). Lithic fragments (19.2 %–80.0 %) comprise dominant metamorphic lithics (mostly metasedimentary lithics, 19.2 %–64.0 %, average: 35.9 %) and carbonate lithics (0–38.4 %, average: 17.1 %), with minor sedimentary and volcanic lithics (Fig. 5). Quartz is the secondary components in most samples and ranges from 17.4 % to 70.2 %. Feldspar content ranges from 2.6 % to 12.9 %, primarily consisting of plagioclase, with small amounts of K-feldspar. These samples are moderately to well

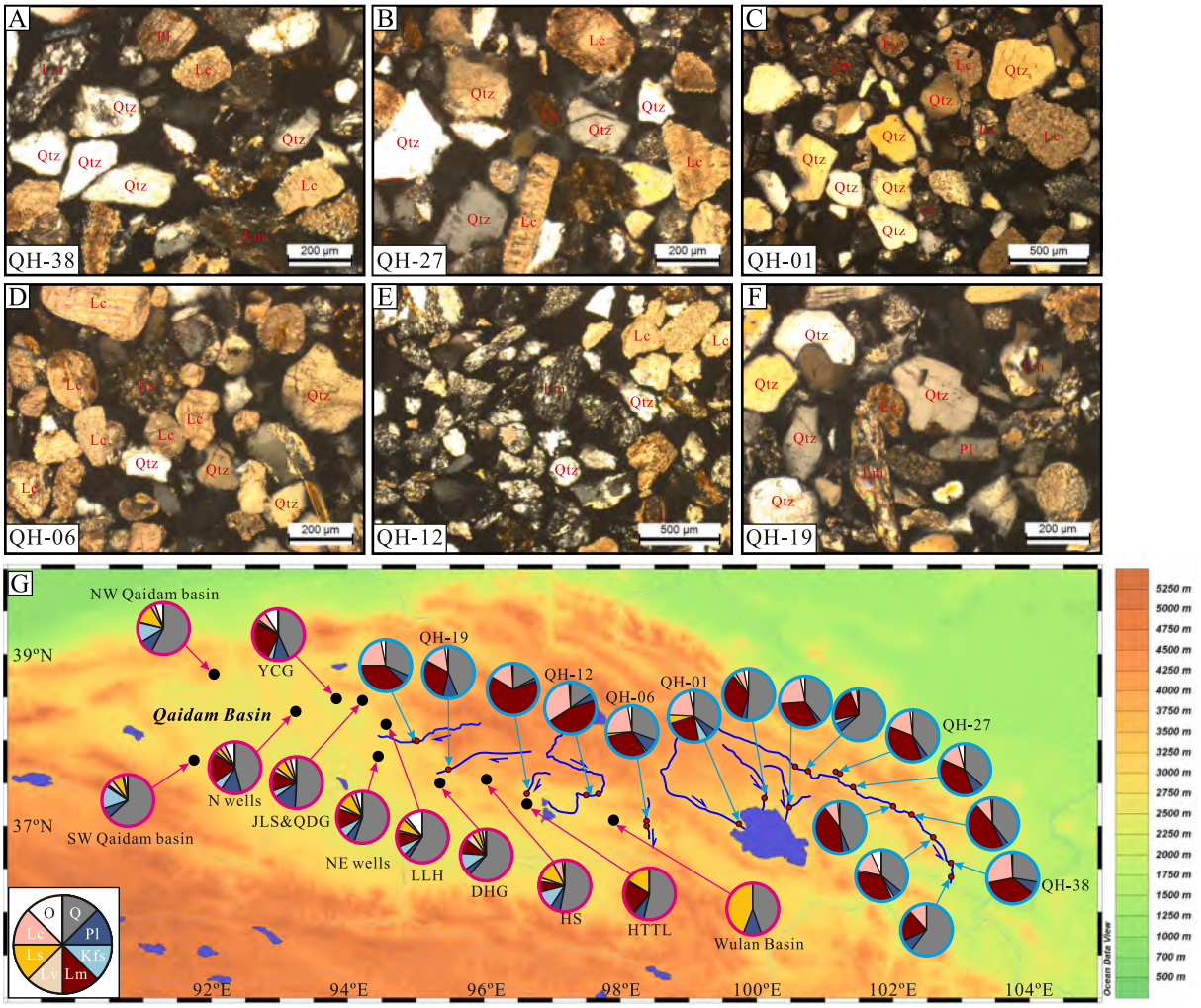

Fig. 5. (A-F) Representative photomicrographs of analyzed river sand samples. (G) Spatial patterns of petrographic compositions of modern river sands and Cenozoic Qaidam Basin sandstones. Compositional data of Cenozoic Qaidam Basin sandstones are average results of all samples in each region. Abbreviations in the figure: Qtz: Quartz; Pl: Plagioclase; Kfs: K-feldspar; Lv: volcanic lithic fragment; Ls: sedimentary lithic fragment; Lm: metamorphic lithic fragment; Lc: carbonate lithic fragment.

sorted and subangular to well rounded (Fig. 5). Notably, quartz grain shapes are diverse, ranging from angular to well rounded, while carbonate lithics grains are mostly rounded (Fig. 5A–F).

4.2. *Conglomerates, paleocurrent orientations and sandstone petrographic features of the studied Cenozoic outcrop sections*

Conglomerates are primarily distributed within the Lulehe, Xia Ganchaigou, Shizigou and Qigequan formations (Fig. 3A–C, I–M), where they occur as interlayers or thick beds, reflecting braided river and alluvial fan sedimentary environments. In the Lulehe Formation, conglomerate beds are both matrix-supported (DHG and LLH sections; Fig. 3A–B) and clast-supported (HS section; Fig. 3C). The conglomerate clasts display a diverse lithological assemblage, including quartzite, metasedimentary rocks, chert, sandstone, mudstone, carbonate, and igneous rocks. Notably, conglomerate clast composition varies among sections. Metamorphic clasts are abundant in the DHG section, while sedimentary clasts are more prevalent in the HS section. Conglomerates are thin interlayer in the Shang Youshashan Formation and are mostly fine gravel (Fig. 3I–J). Thick conglomerate beds in the Shizigou and Qigequan formations are also both matrix- and clast-supported (Fig. 3K–M). The clast compositions in different sections are generally similar, consisting of metasedimentary rocks, carbonate, igneous rocks, and chert.

Paleocurrent measurements in the DHG section reveal a dominant south-directed paleoflow, with the exception of northward direction in the Lulehe Formation (Fig. 4). In the HS section, the Lulehe to Shang Ganchaigou formations exhibit southward paleoflow, while the Qigequan Formation shows a northward direction (Fig. 4).

The Lulehe formation sandstone samples are primarily matrix-supported, poorly to moderately sorted, and subangular to well rounded (Fig. 6A–C). They are predominantly composed of quartz, (meta)sedimentary lithics and feldspar, with an average modal composition of $Q_{52}F_{20}L_{22}$ (Fig. 4). The Xia Ganchaigou Formation samples are clast-supported, with reduced matrix and cement content, and demonstrate moderately to well sorted (Fig. 6D–F). The sandstone compositions in the DHG, LLH and HS sections are similar, characterized by high quartz content (39.6 %–72.9 %) and low lithic fragments content (15.4 %–43.5 %; mainly metamorphic and volcanic lithics). The JLS section samples are primarily composed of quartz and metamorphic lithics (the average modal composition of $Q_{58}F_9L_{31}$). The Shang Ganchaigou Formation sandstones are mostly well sorted and subrounded to well rounded (Fig. 6G–I). The petrographic compositional data indicate that sandstones in the DHG, LLH and HS sections are dominated by quartz (46.9 %–74.8 %) with minor of feldspar, volcanic lithics, metamorphic lithics and mica (Fig. 4). Five samples in the QDG section have lower quartz contents (average Q:F:L ratio of 46:20:28) compared to other sections. Furthermore, fine sandstones in the Shang Ganchaigou

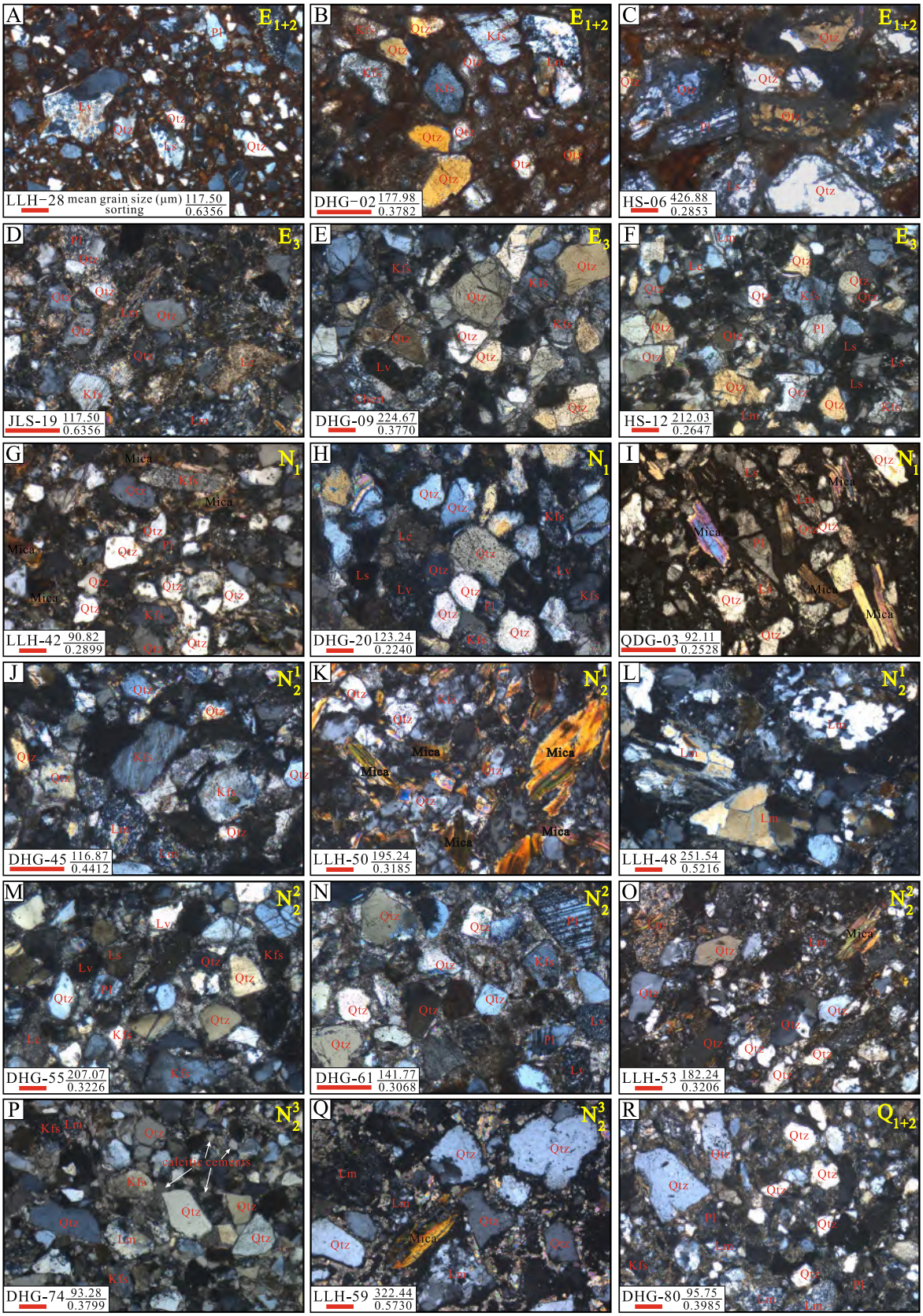

Fig. 6. Representative photomicrographs of analyzed sandstone samples from the Lulehe to Qigequan formations. (A–C): Matrix-supported fine-coarse sandstone in the Lulehe Formation; (D-F): Xia Ganchaigou Formation; (G–I): Shang Ganchaigou Formation, note that the contents of mica in fine-grain samples increase; (J–L): Xia Youshashan Formation; (M–O): Shang Youshashan Formation; (P–Q) Shizigou Formation; (R) Qigequan Formation. Abbreviations in the figure: Qtz: Quartz; Pl: Plagioclase; Kfs: K-feldspar; Lv: volcanic lithic fragment; Ls: sedimentary lithic fragment; Lm: metamorphic lithic fragment; Lc: carbonate lithic fragment. Red bars represent 200 μm. (For interpretation of the references to colour in this figure legend, the reader is referred to the web version of this article.)

Formation are featured by abundant mica and carbonate lithics (Fig. 6I). The Xia Youshashan Formation samples in the DHG section are dominated by quartz (41.4 %–58.5 %) and K-feldspar (9.9 %–37.7 %), with subordinated volcanic and metamorphic lithics (Figs. 4, 6J). Compositions of Xia Youshashan Formation samples in the LLH section are diverse and basically composed of quartz, metamorphic lithics, and mica (Figs. 4, 6K–L). Samples in the Shang Youshashan Formation are mostly moderately sorted and subangular to rounded, but are spatially diverse in compositions (Figs. 4, 6M–O). The average modal composition of samples for the DHG section is $Q_{55}F_{20}L_{19}$, $Q_{52}F_{10}L_{32}$ for the LLH section, and $Q_{40}F_{41}L_{12}$ for the QDG section. Coarse sandstones in the Shizigou and Qigequan formations are poorly sorted and angular to rounded (Fig. 6P–R). These samples are dominated by quartz (46.2 %–80.1 %) with subordinated K-feldspar (7.1 %–23.8 %) and metamorphic lithics (6.2 %–27.1 %; Fig. 4).

All measured grains are mostly very fine sand to medium sand (Fig. 6), grain sizes of which range from 32.57 to 857.84 μm, with an average of 161.03 μm. The mean grain sizes of samples from the DHG section range from 57.61 to 253.85 μm (average: 149.33 μm), while that of the LLH section ranges from 82.53 to 341.79 μm (average: 174.75 μm). The mean grain sizes of samples HS-06, JLS-19, HS-12, and QDG-03 are 426.88, 117.50, 212.03, and 92.11 μm, respectively. The sorting indices of all analyzed samples range from 0.2220 to 0.8158 (Fig. 6), with an average of 0.3867. The average sorting of all samples from the LLH section is 0.4341, which is higher than that of all samples from the DHG section (0.3564). Samples from the Lulehe Formation are relatively poor-sorted with high sorting index (average: 0.4789; Fig. 6A–C). All analyzed grains are mostly subrounded to well rounded, with an average quantified roundness of 0.6344 (maximum: 0.9998 and minimum: 0.1912). The average roundness of samples from the DHG section ranges from 0.5406 to 0.7214 (average: 0.6348), and from 0.5822 to 0.7310 (average: 0.6315) in the LLH section.

4.3. Petrographic composition of Cenozoic sandstones from the entire Qaidam Basin

A total of 599 petrographic data of Cenozoic sandstone were compiled in our dataset, including 339, 154, 31, and 75 from the northern, northeastern, northwestern, and southwestern regions, respectively. Petrographic data indicate that the Cenozoic Qaidam Basin sandstone have spatially diverse compositions (Fig. 7). The petrographic compositions of northern Qaidam Basin samples are of large variety and are mostly lithic arkose and feldspathic litharenites (Fig. 7B). These samples are mainly plotted in the recycled orogen, mixed and arc fields in the Qm-F-Lt ternary (Fig. 7A) (Dickinson, 1985). Northeastern Qaidam Basin sandstones are dominantly feldspathic litharenites and subordinately litharenites and lithic arkose (Fig. 7B), and are mostly plotted in transitional recycled orogenic, mixed and transitional continental block fields (Fig. 7A–B). The modal compositions of samples from the northwestern and southwestern Qaidam Basin are quite similar and are mainly lithic arkose with small amounts of arkose samples (Fig. 7B). Western Qaidam Basin samples are dispersedly scattered in transitional continental block, mixed, quartzose recycled orogen fields (Fig. 7A), despite the numbers of data are limited because of lacking of Qm-F-Lt data in some literatures. The Lm-Lv-Ls + Lc ternary indicate that sandstones in the northern and northeastern Qaidam Basin are characterized by high content of metamorphic lithics, whilst samples from southwestern basin are dominated by volcanic lithics and northwestern basin are dominated by sedimentary lithics (Fig. 7C).

4.4. Spatial variations in sandstone petrographic composition of each stratigraphic unit

The Lulehe Formation samples collected from seven sections or regions are mainly located in the north edge of the Qaidam Basin. Most Lulehe formation sandstones are matrix-supported with high contents of cement and matrix (ranging from 5.7 % to 65.4 % in 27 samples, average: 27.3 %), consistent with alluvial sedimentary environment. Petrographic data reveal minor compositional variation among different areas (Fig. 8A). Sandstones from the northeastern Qaidam Basin are featured by (meta)sedimentary lithics and high contents of quartz and feldspar. In contrast, samples in the EBL and LH.7 regions exhibit lower quartz and lithic contents. Samples from the HSH section, representing northwestern Qaidam Basin, contain more quartz and fewer lithic fragments (mainly sedimentary lithics) compared to samples from other regions.

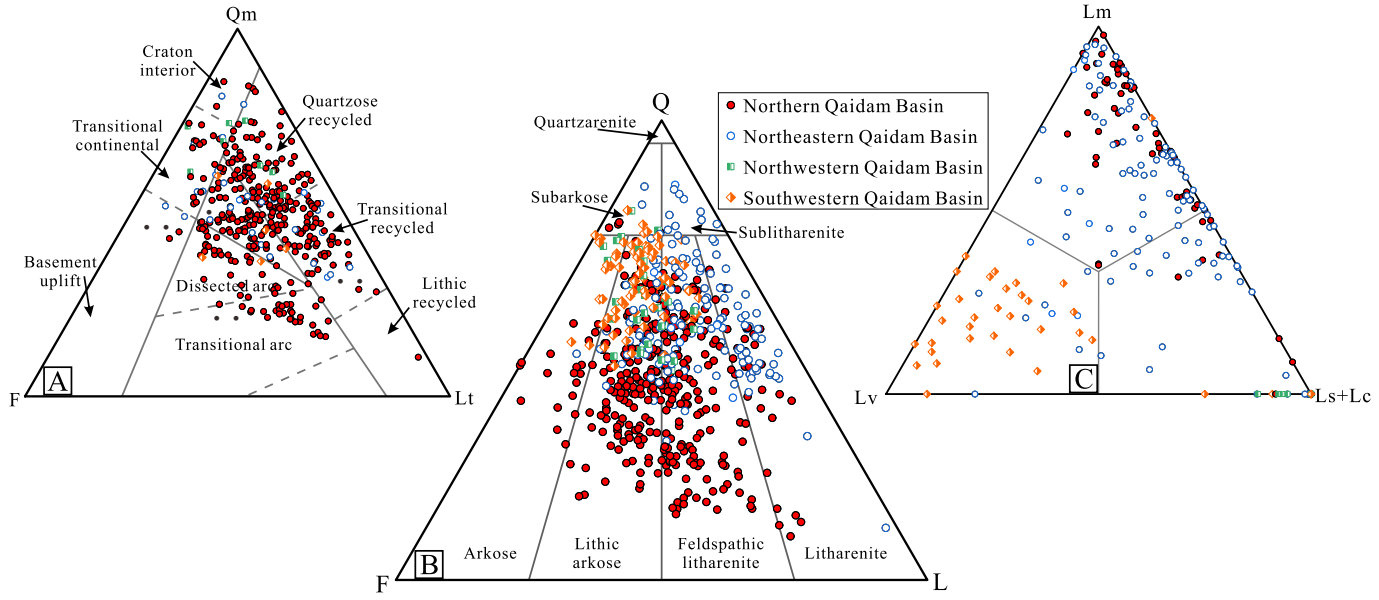

Fig. 7. Ternary diagrams of petrographic composition of sandstones from the Cenozoic Qaidam Basin. (A) Qm-F-Lt diagram for discriminating tectonics of source region following Dickinson (1985). 1. Continental block; 2. Recycled orogen; 3. Magmatic arc. (B) Q-F-L diagram for sandstone classification following Folk (1980). (C) Lithic fragment assemblage Lm-Lv-(Ls + Lc). Abbreviation in the figure: Qm: monocrystalline quartz; Q: including Qm and polycrystalline quartz (Qp); F: total feldspar grains including plagioclase and K-feldspar; Lt: total lithic fragments including Qp, Lm, Lv, Ls, and Lc. L: total unstable lithic fragments including Lm, Lv, Ls and Lc.

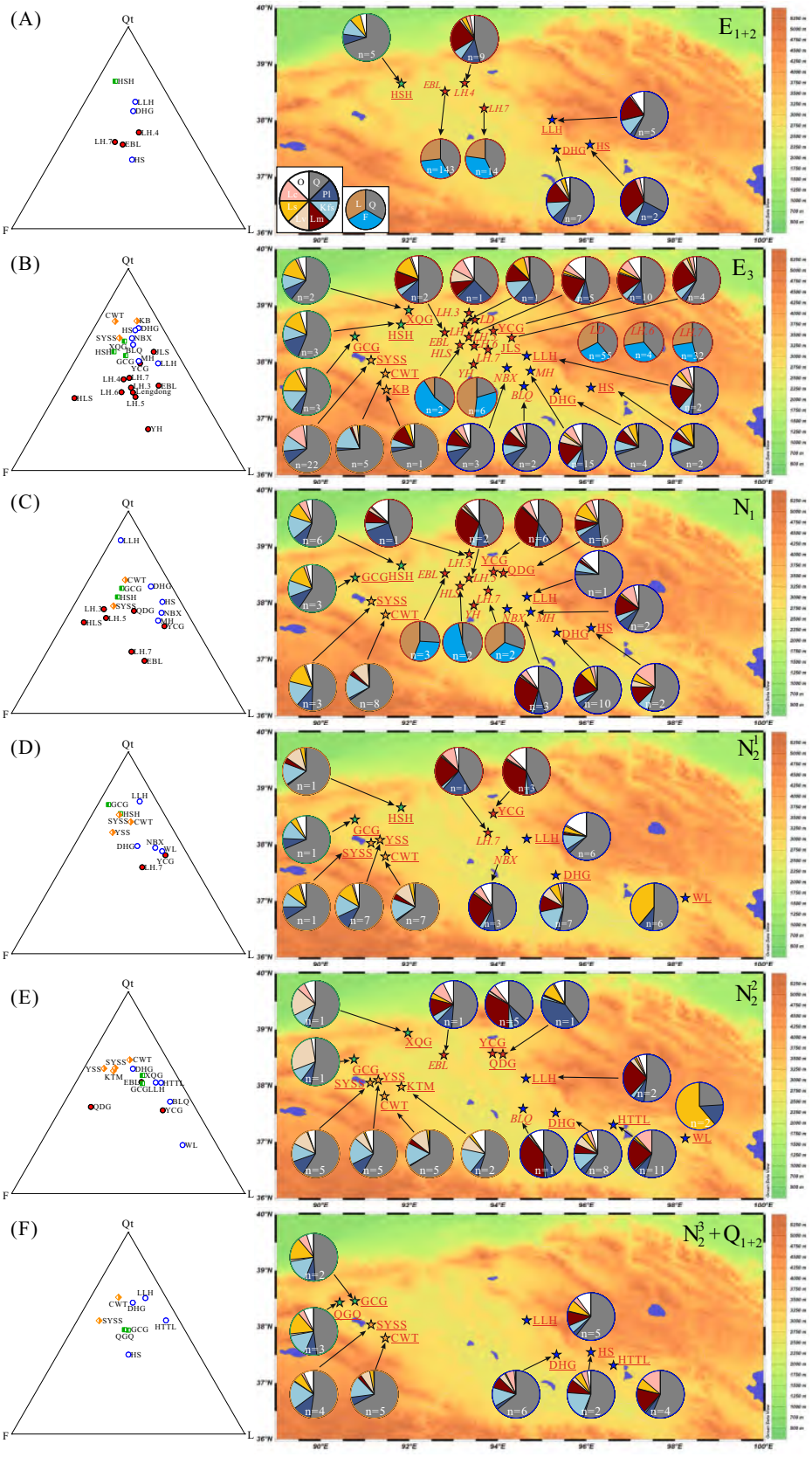

Fig. 8. Spatial patterns of petrographic composition of the Cenozoic Qaidam Basin sandstones in each formation. Note that petrographic data of samples in the southeastern margin of Qaidam Basin is lack. Lacking well-exposed outcrop (Liu et al., 2008; Bao et al., 2017) and secondary role of Cenozoic strata in hydrocarbon exploration (Pang et al., 2005; Zhang et al., 2018) in the southeastern Qaidam Basin may be the reason.

The Xia Ganchaigou Formation samples are widely distributed along the current margins of Qaidam Basin and show significant compositional variability (Fig. 8B). Overall, the northern Qaidam Basin shows greater variation among different sections or region (Fig. 8B). Samples in the northern basin are characterized by relatively low quartz contents (mostly below 50 %), but vary in contents of lithic fragments (mainly metamorphic and carbonate lithics). Samples from the YCG, JLS sections, as well as LH.5 region, where are proximal to the Qilian Mountains, contain higher proportions of metamorphic lithics than those from other regions. In contrast, samples from the northeastern Qaidam Basin exhibits less compositional variability than those from the northern basin, and are quartz-rich with secondary of metamorphic lithics and feldspar. Three sections in the northwestern Qaidam Basin display highly similar sandstone petrographic compositions, consisting mainly of quartz, feldspar, and sedimentary lithics. The Q:F:L ratios of sandstones from three sections in the southwestern basin are similar with those in the northwestern basin, while lithic fragments in the SYSS region are dominated by carbonate lithics, metamorphic lithics in the KB section, and volcanic lithics in the CWT section.

Petrographic patterns of the Shang Ganchaigou and Xia Youshashan formation samples are similar with the Lulehe Formation samples (Fig. 8C–D). Samples in the northeastern Qaidam Basin display evident spatial variation, with notably higher quartz content compared with those from the northern basin. However, metamorphic lithics are a secondary component in both northern regions. Samples in the western Qaidam Basin are quite uniform in composition and consist of quartz, K-feldspar, and sedimentary lithics. The Shang Youshashan Formation sandstones in the northern and northeastern basin to some extent inherited petrographic composition from the Xia Ganchaigou and Shang Ganchaigou formation samples, and indicate slightly spatial variation (Fig. 8E). Additionally, samples from the Wulan Basin, as a small basin located at the eastern edge of the Qaidam Basin (Fig. 1), are sedimentary lithics-rich with high quartz content. Furthermore, mica is an important component in these samples, despite the content of mica varies spatially (Fig. 8E).

The coarse sandstones from Shizigou and Qigequan formations are mainly distributed in the western and northeastern Qaidam Basin (Fig. 8F). These samples are quartz-rich but differ in the lithic types. Sedimentary and metamorphic lithics are major lithic types in the northeastern samples while sedimentary lithic is dominating in the western basin samples.

4.5. Temporal variations in sandstone petrographic composition of the major depositional areas

Sandstone petrographic compositions from different depositional areas indicate diverse temporal trends (Fig. 8). In the northern Qaidam Basin, the average content of quartz remains relatively stable over time, but the Lulehe and Xia Ganchaigou formation samples display a wider range of quartz content than those from other strata. Feldspar content progressively decreases and lithics content increases from the Lulehe to Shang Youshashan formations. Specifically, the proportions of metamorphic lithics and mica are higher in the Shang Ganchaigou, Xia Youshashan, and Shang Youshashan formation samples. Similarly, quartz content in northeastern Qaidam Basin shows no significant temporal variation from the Lulehe to Qigequan formations. However, feldspar content decreases, while lithic content increases above the Lulehe Formation. The two dominant lithic types, i.e., sedimentary and metamorphic lithics, show no evident temporal trend. Carbonate lithic contents are highest in the Xia Ganchaigou samples and decreases upward. In the western Qaidam Basin, petrographic compositions reveal a distinct trend. Quartz content decreases, while feldspar, and lithic and mica contents increase from the Lulehe to Qigequan formations.

5. Discussion

5.1. Provenance of the Cenozoic Qaidam Basin sandstones

Both previously reported and new petrographic data demonstrate significant spatial and temporal variations in the composition and texture of Cenozoic sandstones within the Qaidam Basin (Figs. 6, 7, 8). These differences suggest varying sources for sandstone across different regions and stratigraphic units. Provenance interpretations and potential relationship with the Cenozoic tectonics and climate are stated as follows.

5.1.1. Northern Qaidam Basin

Sandstones in the northern Qaidam Basin are relatively immature (Fig. 8) and exhibit diverse petrographic compositions. The Q-F-L ternary diagram reveals dominating recycled orogen sources, with minor contributions from magmatic arcs (Fig. 6). Diverse petrographic compositions indicate mixed provenance from metamorphic rocks, igneous rocks and recycled (meta)sedimentary exposed in the Qilian Mountains and the Altun Range. Consistent with these observations, heavy mineral assemblages are dominated by garnet and epidote, with minor zircon and tourmaline (Jian et al., 2013a), indicating predominant contributions from the metamorphic rocks and subordinate intermediate-acid igneous rocks. Detrital garnet trace element geochemical data further emphasize the dominant contribution from the North Qaidam metamorphic belt (Hong et al., 2020).

The Lulehe Formation samples from the EBL, LH.4, and LH.7 regions exhibit comparable average model compositions (Fig. 8A), while considerable compositional variability is observed within each region (Fig. 7). This variability may reflect an unstable source-to-sink system, possibly indicative of a tectonically-active setting. The widespread thick conglomerates (consist of various metasedimentary clasts and subordinate granite clasts) in the Lulehe Formation, coupled with seismic profile evidences, suggest a high-gradient depositional system with proximal sources (the South Qilian and North Qaidam terranes) (Zhuang et al., 2011; Cheng et al., 2019a; Jian et al., 2023). The Xia Ganchaigou Formation sandstones are compositionally similar to those of the Lulehe Formation (Fig. 8B), implying consistent sediment supply from the South Qilian and North Qaidam terranes. However, the Xia Ganchaigou Formation samples display greater spatial variability in composition (Fig. 8B), which contrasts with the homogeneous detrital zircon age populations (Jian et al., 2024). The expansion of the paleo-Qaidam lake during the deposition of Xia Ganchaigou Formation (Zhuang et al., 2011; Cheng et al., 2019b, 2021) may explain the well mixed zircon age signals (Jian et al., 2024). Notably, the Xia Ganchaigou Formation samples span a wide area (Fig. 8), with varying distances to the hinterland of the North Qaidam and South Qilian terranes. We infer that these distance differences, combined with the low-gradient depositional conditions (Zhuang et al., 2011), contributed to the observed petrographic heterogeneity. The Shang Ganchaigou Formation samples inherit compositional features from both the Lulehe and Xia Ganchaigou formations and also show spatial diversity, with an average modal composition of $Q_{42}F_{27}L_{28}$ (Figs. 8, 9). This consistency suggests minimal change in sediment sources during this tectonically-quiet period (Zhuang et al., 2011; Bao et al., 2017). In contrast, the overlying Xia Youshashan and Shang Youshashan formation sandstones show higher lithic content, specifically metamorphic lithics, and lower feldspar content (Fig. 9). These differences align with the increasing proportions of Precambrian detrital zircon in the northern Qaidam Basin sandstones (Jian et al., 2024), pointing to enhanced contributions from meta(sedimentary) strata in the South Qilian terrane. This shift in provenance may be attributed to crustal shortening in the northern Tibetan Plateau since the Miocene (Bovet et al., 2009; Zhuang et al., 2011; Cheng et al., 2019b). Additionally, the detrital mica content of samples in the Shang Ganchaigou to Shang Youshashan formations is significantly higher than those in the Lulehe and Shang Ganchaigou formations (Fig. 9), likely due

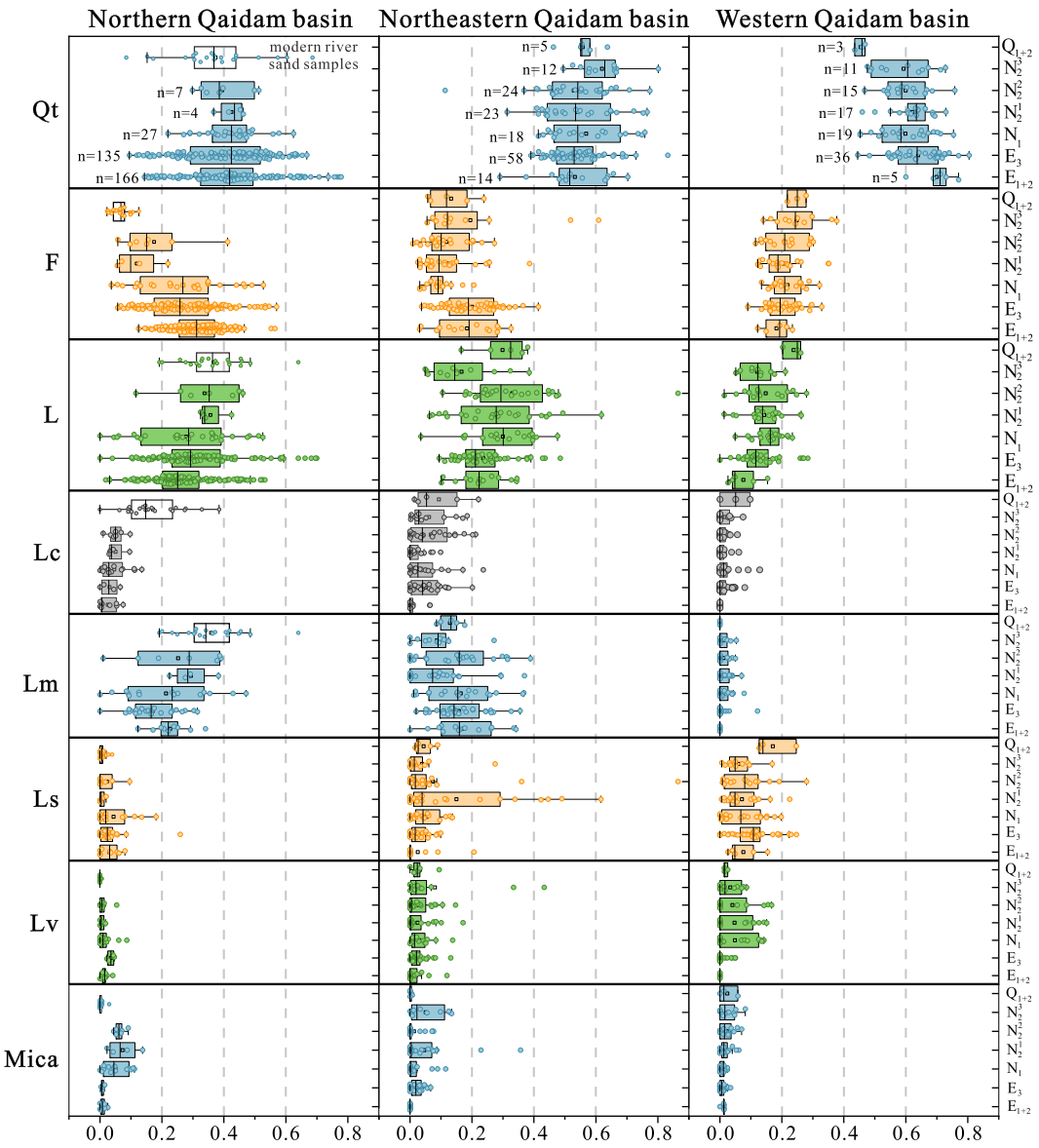

Fig. 9. Box-plots of petrographic compositions of samples in each formation from different regions. Petrographic composition of modern river sand samples are also plotted marked by unfilled box. Abbreviation in the figure: Qt: total quartz grains; F: total feldspar grains; L: total unstable lithic fragments including Lm, Lv, Ls and Lc; Lc: carbonate lithic fragment; Lm: metamorphic lithic fragment; Ls: sedimentary lithic fragment; Lv: volcanic lithic fragment.

to smaller grain size and preferential deposition of mica in relatively fine-grained fractions (Ye et al., 2024). While petrographic data are unavailable for the Shizigou and Qigequan formations, detrital zircon U-Pb geochronological results reveal similar spatial variations and a consistent provenance from the adjacent Qilian Mountains (Jian et al., 2024). Collectively, these findings demonstrate continuous sediment supply to the northern Qaidam Basin from the South Qilian and North Qaidam terranes.

5.1.2. *Northeastern Qaidam Basin*

The sandstones in the northeastern Qaidam Basin are generally characterized by higher quartz content and greater compositional maturity than those in the northern basin (Fig. 7A). Most samples are plotted within the recycled and mixed fields on the Q-F-L ternary diagram (Fig. 7). Stratigraphically, the Lulehe Formation sandstones in the northeastern Qaidam Basin are mostly matrix-supported and poorly sorted with angular to subangular grains (Fig. 6A–C), suggesting proximal sediment sources and high-relief environments (Jian et al., 2023). Petrographic compositions are slightly various and dominated by quartz and low-grade metasedimentary lithics (classified as sedimentary lithics in Jian et al., 2023), except that content of quartz in the HS section is lower. Detrital zircon U-Pb age populations in the Lulehe Formation sandstones are characterized by dominant Early-Paleozoic and subordinate Precambrian ages, revealing derivation from the Neoproterozoic basement rocks in the Qilian Mountains and the Qaidam pre-Cenozoic basement (Cheng et al., 2019b; Jian et al., 2024). We therefore infer that the adjacent North Qaidam and South Qilian terranes were the primary sources during the deposition of Lulehe Formation. This conclusion contrasts with the interpretation that the Eastern Kunlun Range was the major source based on the eastward paleocurrent orientations and the presence of Permian–Triassic detrital zircon ages (Bush et al., 2016; Wang et al., 2017). The Xia Ganchaigou Formation samples are generally grain-supported (Fig. 6E–F) and inherit petrographic compositions from the Lulehe Formation. Minor spatial variations (Figs. 8, 9) likely reflect a transition from a high-relief alluvial to low-gradient fluvio-lacustrine environment (Zhuang et al., 2011; Guan and Jian, 2013) without significant sedimentary sources changes. Notably, carbonate lithics are important framework detrital components

in samples from LLH and DHG sections and MH region (Fig. 8), suggesting contributions from the carbonate strata within the North Qaidam and South Qilian terranes. Petrographic data from the Lulehe to Shang Ganchaigou formations show a notable trend of decreasing feldspar and increasing lithic contents (Fig. 9), implying enhanced input from metamorphic rocks since the deposition of the Shang Ganchaigou Formation. We argue that this reflects variable contributions from different parent-rocks within the South Qilian and North Qaidam terranes, rather than a shift in provenance from the North Qilian to the South Qilian and North Qaidam terranes (Bush et al., 2016). Sandstones from the Shang Ganchaigou, Xia Youshashan, and Shang Youshashan formations are compositionally similar, characterized by high quartz content and abundant metamorphic lithics and mica, indicating stable sources during this period (Figs. 7, 8). The overlying Shizigou and Qigequan formation sandstones mark a distinct compositional shift toward greater maturity and reduced metamorphic lithics (Fig. 8), indicating increasing contributions from recycled sedimentary strata. Li et al. (2021) proposed a source shift from the Eastern Kunlun Range to the Qilian Mountains during this period, based on increasing carbonate lithics, negative shift in εNd values, and increase in Precambrian zircon grains recorded in the HTTL section. However, our petrographic data show consistently high proportions of metamorphic and carbonate lithics throughout the Cenozoic (Fig. 9), affirming continuous contributions from the Qilian Mountains. Additionally, sandstones in the Wulan basin (Fig. 8D–E) mainly consist of quartz and sedimentary lithics (Li et al., 2023), differing from other sections in the northeastern Qaidam Basin. This distinct composition implies different sources and isolated depocenters in the Wulan basin, likely resulting from local deformation within the North Qaidam belt (Li et al., 2023).

Our results demonstrate that the northeastern Qaidam Basin was continuously supplied by the Qilian Mountains, challenging previous detrital zircon-based interpretations that the Eastern Kunlun range dominantly fed the northeastern Qaidam Basin in early period of Lulehe Formation (Bush et al., 2016; Wang et al., 2017) or prior to the deposition time of Shizigou Formation (Li et al., 2021). The limited contribution from the Eastern Kunlun Range to the northeastern Qaidam Basin can be explained as follows. First, regarding the 240–270 Ma age cluster as diagnostic signature of the Eastern Kunlun Range (e.g., Bush et al., 2016; Wang et al., 2017), due to the high proportion of Permian–Triassic plutons in the Eastern Kunlun Range (40 %; Fig. 1C), is inappropriate. Because the contribution from Permian–Triassic plutons in the North Qaidam terrane has been underestimated, as they constitute 16.8 % in the modern North Qaidam UHP belt (Fig. 1C). In addition, Jian et al. (2024) proposed that Paleoproterozoic ages (i.e., 1800–2000 Ma and 2350–2500 Ma) can serve as a distinctive indicator to distinguish sources from the Qilian Mountains, the Altun and Eastern Kunlun ranges. Second, grain textural bias may influence detrital zircon age distributions. Phanerozoic zircon grains preferentially concentrate in coarse-grained fractions (125–250 μm), whereas older Precambrian zircon grains are more abundant in fine-grained fractions (32–125 μm) (Shen et al., 2024). This pattern is because that older recycled zircon grains tend to be more rounded and thus to be smaller than younger grains which underwent fewer recycling (Yang et al., 2012; Resentini et al., 2018). Third, metamorphic rock-sourced signals are found in most samples from the northeastern Qaidam Basin. For instance, metamorphic lithic fragments are commonly dominant components in all samples from the northeastern Qaidam Basin (Fig. 8). In addition, high content of garnet and epidote in heavy mineral assemblages (Jian et al., 2013a; Fu et al., 2022), granulite-facies metapelites-sourced detrital garnet (Hong et al., 2020), and dominant early Paleozoic and minor Precambrian detrital zircon ages (Jian et al., 2024), collectively indicate that metamorphic rocks are the major sources. Overall, we propose that the northeastern Qaidam Basin represents a relatively uniform source-to-sink system, with minor spatial variations primarily controlled by varying contributions from different parent-rocks in the Qilian Mountains.

5.1.3. Western Qaidam Basin

Sandstones in the western Qaidam Basin (including northwestern and southwestern regions) exhibit distinct compositional differences compared to those in the eastern basin (Fig. 7). The northwestern basin, closed to the south flank of the Altun Range, contains moderately sorted sandstones which are characterized by high quartz content and a substantial proportion of feldspar (Fig. 7). Lithic fragments are relatively minor and are mainly clastic sedimentary and carbonate lithics (Figs. 7, 8). In the southwestern Qaidam Basin, adjacent to west part of Eastern Kunlun Range (Qimantagh region), sandstones have similar quartz and feldspar contents, but volcanic lithics are major lithics type in these sandstones (Fig. 7). Petrographic compositions suggest that western Qaidam Basin sandstones were primarily derived from the Jurassic clastic sedimentary strata and Precambrian carbonate rocks in the south flank of Altun Range and igneous rocks in the Qimantagh region (Rieser et al., 2005; Xia et al., 2021). This is consistent with provenance interpretation based on paleocurrent orientation, heavy mineral assemblage and detrital zircon U-Pb geochronology (Cheng et al., 2016a; Zhu et al., 2017; Zhou et al., 2018; Xia et al., 2021; Jian et al., 2024). Petrographic data from the western Qaidam Basin also indicate temporal variations in sandstone composition (Fig. 9), likely reflecting the uplift and exhumation histories of the Altun and Eastern Kunlun ranges, as well as the Qimantagh region (Cheng et al., 2016a, 2019a; Zhou et al., 2018; Xia et al., 2021).

In summary, basin-wide petrographic compositional data, integrated with other provenance indices, demonstrate that sediments from different areas of the Qaidam Basin were primarily derived from the adjacent mountains (Table 1). The South Qilian and North Qaidam terranes, rather than the Eastern Kunlun Range, served as the dominant sources for Cenozoic sediments in the northeastern and northern Qaidam Basin. Notably, temporal variations in petrographic composition reflect changing contributions from metamorphic rocks, plutons and recycled sedimentary strata in the Qilian Mountains. In contrast,

Table 1
Provenance signatures and interpretations of the Cenozoic Qaidam Basin sandstones.

Provenance signatures	Northern Qaidam Basin	Northeastern Qaidam Basin	Western Qaidam Basin
Petrographic compositions [a]	$Q_{39}F_{28}L_{28}$; Metamorphic lithics-dominated	$Q_{46}F_{13}L_{23}$; Metamorphic lithics-dominated	$Q_{52}F_{18}L_{12}$; Volcanic and sedimentary lithics-dominated
Heavy mineral assemblages [b]	Garnet-epidote-zircon-tourmaline	Garnet-epidote-zircon	Zircon-Hornblende-epidote-garnet
Detrital zircon U-Pb geochronology [c]	400–480 Ma; Precambrian; 220–280 Ma	400–480 Ma; Precambrian; 220–280 Ma	400–480 Ma; 220–280 Ma
Detrital muscovite $^{40}Ar/^{30}Ar$ geochronology [d]	300–400 Ma	300–400 Ma	200–300 Ma; 300–500 Ma
Detrital single mineral geochemistry [e]	Metapelites-sourced garnet; Metapelite-sourced tourmaline	Metapelites-sourced garnet; Metapelite and granitoid-sourced tourmaline	High grade metamorphic rocks-sourced garnet; Metapelite and granitoid-sourced tourmaline
Source terranes	Qilian Mountains-dominated	Qilian Mountains-dominated	Eastern Kunlun and Altun ranges-dominated

[a] Modal composition represents average of all samples in the region.
[b] Major heavy mineral species, data from Jian et al., 2013a, Zhu et al., 2017.
[c] Common feature of detrital zircon U-Pb geochronological populations, temporal and spatial variations of which is reviewed in Jian et al., 2024.
[d] Dominating detrital muscovite age clusters (reviewed by Ye et al., 2024).
[e] Detrital single mineral geochemistry-based interpretations from Jian et al., 2013a, Li et al., 2018; Hong et al., 2020.

sediments in the western Qaidam Basin were mainly sourced from the Altun Range and western segment of the Eastern Kunlun Range.

5.2. Factors controlling the sandstone petrographic composition and texture

5.2.1. Tectonics and parent-rock lithology

The Qilian Mountains and the Eastern Kunlun Range have fundamentally distinc tectonic histories, which have led to pronounced lithological differences. The Qilian Mountains documents the assembly and breakup of the Rodinia and Pangea supercontinents (Zhang et al., 2021), while the Eastern Kunlun Range primarily records the closure of the Proto-Tethys and Paleo-Tethys Oceans. Parent-rock lithology, associated with distinct textural parameters and mineral assemblages, exerts a primary control on the petrographic composition of sand or sandstone (Caracciolo et al., 2012a, 2012b; Garzanti, 2019; Caracciolo, 2020; Johnson et al., 2022). The significant compositional contrast between sandstones in the western and eastern Qaidam Basin highlights the dominant influence of parent-rock lithology. Granitoids are considered highly efficient sand producers and have a sand generation index (SGI) 14–20 times greater than that of low- and medium-grade metamorphic rocks (Palomares and Arribas, 1993). This difference is evident in our study. The high abundance of metamorphic lithics (mostly metasedimentary lithics) in the northern (average: 27.5 %) and northeastern Qaidam Basin (average: 22.6; Fig. 7) suggests that low-medium grade metamorphic rocks, which comprise 32 % of the South Qilian and North Qaidam terranes (Fig. 1), are major sediment sources. In addition, the elevated contents of quartz and feldspar imply significant contributions from intermediate-acid plutons (19 % in the Qilian Mountains) and recycled sedimentary strata (26 % in the Qilian Mountains). Thus, sandstones from the northern and northeastern Qaidam Basin represent mixture of dominating metamorphic rock, intermediate-acid plutons and recycled sedimentary rocks. In contrast, sandstones in the western Qaidam Basin are enriched in quartz and feldspar, with minor sedimentary and volcanic lithics (Fig. 7), indicating sources from intermediate-acid plutons and recycled sedimentary strata from the Altun and Eastern Kunlun ranges (Fig. 1C). Because sands derived from intermediate-acid igneous rocks and metamorphic rocks differ in petrographic composition (Palomares and Arribas, 1993), the quartz/feldspar (Q/F) and lithic/(quartz + feldspar) (L/(Q + F)) ratios to some extent (for instance, when climatic influences are minor) could be used to distinguish contributions from intermediate-acid plutons and metamorphic rocks. The contrast in L/(Q + F) ratios between eastern and western Qaidam Basin sandstones (Fig. 10) reflects differing source lithologies. Furthermore, lower Q/F ratios in the northern Qaidam Basin samples compared to those in northeastern basin (Fig. 11) may reflect the influences of granitic plutons in the west part of the North Qaidam belt (Fig. 1). Additionally, the fluctuant Q/F ratios in samples from the DHG and LLH sections (Fig. 12) indicate varied contributions from plutonic rocks and (meta)sedimentary strata.

5.2.2. Climate and sedimentary environment

Climate influences petrographic composition primarily by promoting the decomposition of relatively unstable components (e.g., carbonate lithics, mica, plagioclase, K-feldspar) under relatively intense chemical weathering conditions. The Qaidam Basin experienced two humid to arid transitions during the Cenozoic (Miao et al., 2013; Song et al., 2013; Bao et al., 2017). Take the DHG section as an example, the Q/F ratios are higher in the Shang Ganchaigou and Shizigou formations (Figs. 11, 12), coinciding with cold and arid climatic conditions (Bao et al., 2017). The anomalous increase in Q/F ratios during periods of relatively weak weathering suggests that climate may play a secondary role in controlling sandstone modal composition. Additionally, mica and carbonate lithic contents in Cenozoic Qaidam Basin sandstones show an increasing trend (Fig. 9), which may be related to the progressive aridification of the climate (Rieser et al., 2005).

Sedimentary environment also plays a critical role by determining the hydrodynamic conditions during deposition, which in turn influences sediment texture (e.g., grain size and sorting) and affects composition (Garzanti et al., 2008, 2009; Garzanti, 2019). The Cenozoic Qaidam Basin contains thick nonmarine deposits, including alluvial, fluvial, deltaic, and lacustrine sediments (Fig. 2). The sandstones analyzed in this study have different occurrences in the investigated sedimentary strata, including interlayers in conglomerates, thick sandstones, interlayers in siltstones or mudstones (Fig. 3). Grain size and sorting marked variability in the DHG and LLH sections (Fig. 12). For example, alluvial samples from the Lulehe Formation in both sections are poorly sorted (sorting indices >0.4; Fig. 12). Lithic fragments, such as quartzite lithics, commonly have large grain size (Fig. 6L), and the quartz/lithics (Q/L) ratio could thus be influenced by analyzed sample grain size (Caracciolo et al., 2012a). Indeed, the Q/L ratio exhibits a negative correlation with both average grain size and sorting of samples

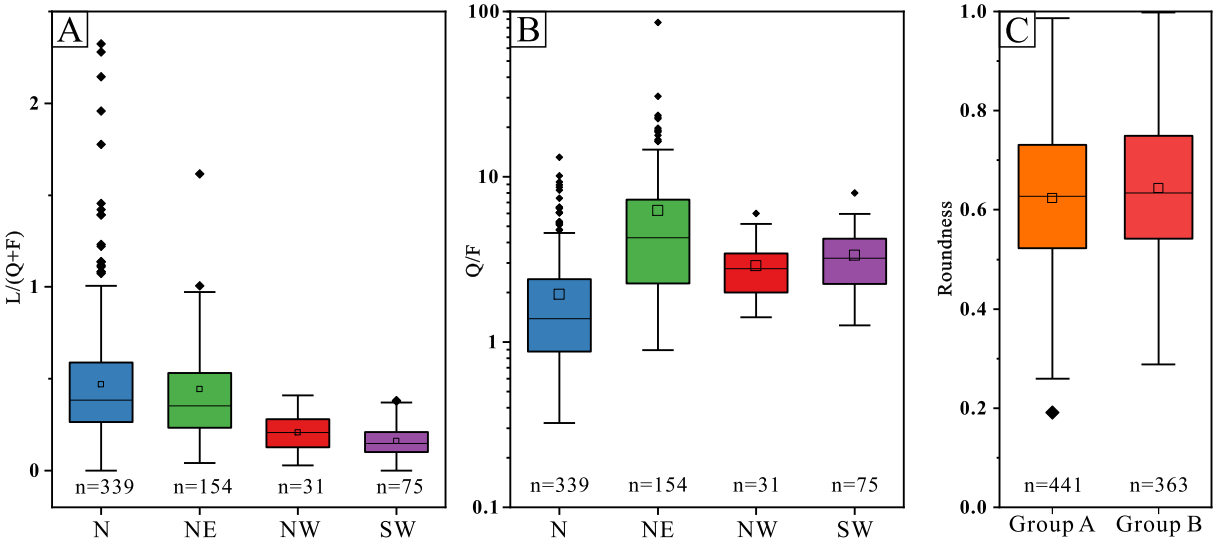

Fig. 10. Box-plots of lithic/(quartz + feldspar) (A) and quartz/feldspar (B) ratios in different regions. (C) Box-plots of roundness of analyzed grains in two groups. Group A represents all grains from samples in DHG section which have more contributions from recycled strata, while Group B represents grains from samples that have less contribution from recycled strata. n represent number of plots.

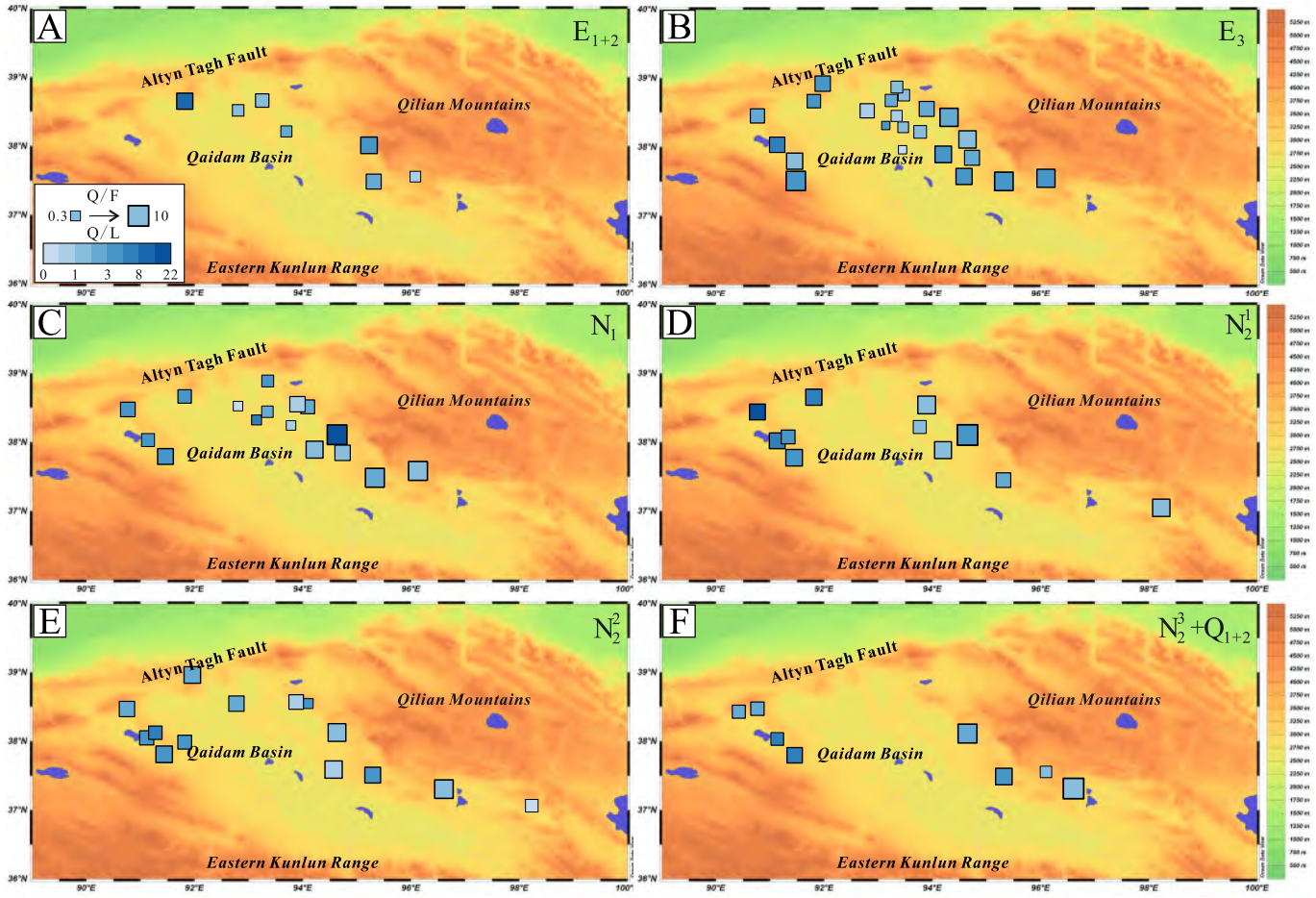

Fig. 11. Hotpot plots of quartz/feldspar (Q/F) and quartz/lithic (Q/L) ratios of Cenozoic Qaidam Basin sandstones. The sizes of squares represent quartz/feldspar ratio and quartz/lithic ratio is reflected by the colour.

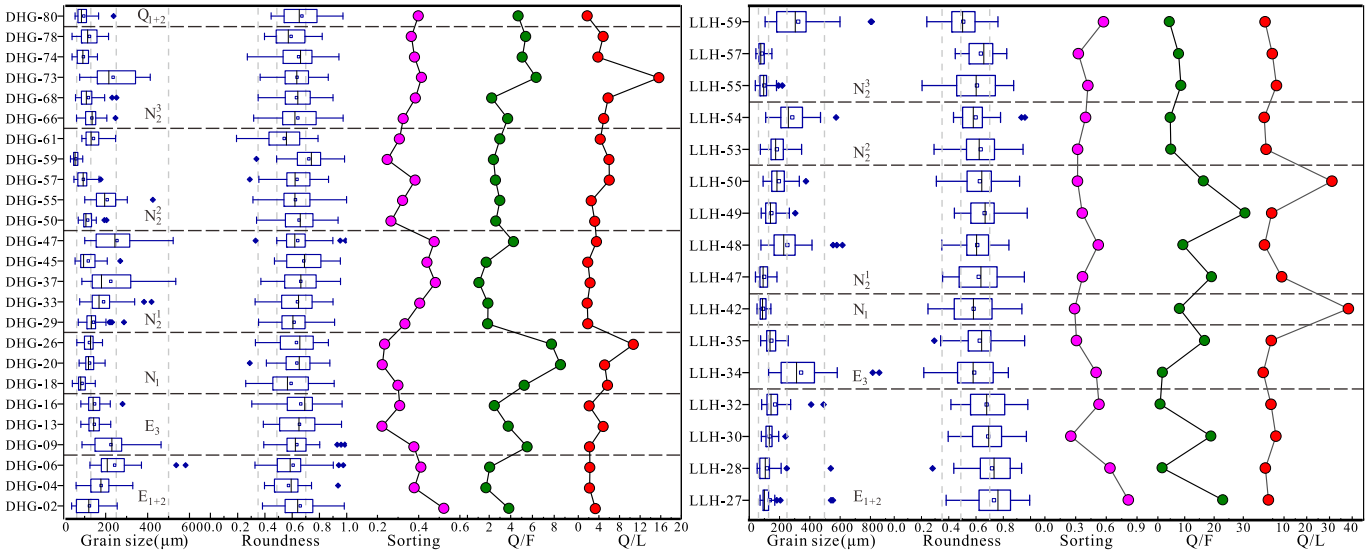

Fig. 12. Vertical variations in grain size, roundness, sorting, quartz/feldspar and quartz/lithic ratios of analyzed samples from the DHG (left panel) and LLH (right panel) sections.

in the DHG and LLH sections (Fig. 13A), highlighting the influence of sediment texture and sedimentary environment on sandstone composition. However, at the basin-wide scale, the Q/L ratios show no clearly spatial patterns (Fig. 10), which may reflect the secondary influence of sedimentary environment on the sandstone composition. Furthermore, abundant mica is observed in samples from the Shang Ganchaigou, Xia Youshashan and Shang Youshashan formations in the northeastern Qaidam Basin (Fig. 6I, K, O; Fig. 9), during the expansion of the Qaidam

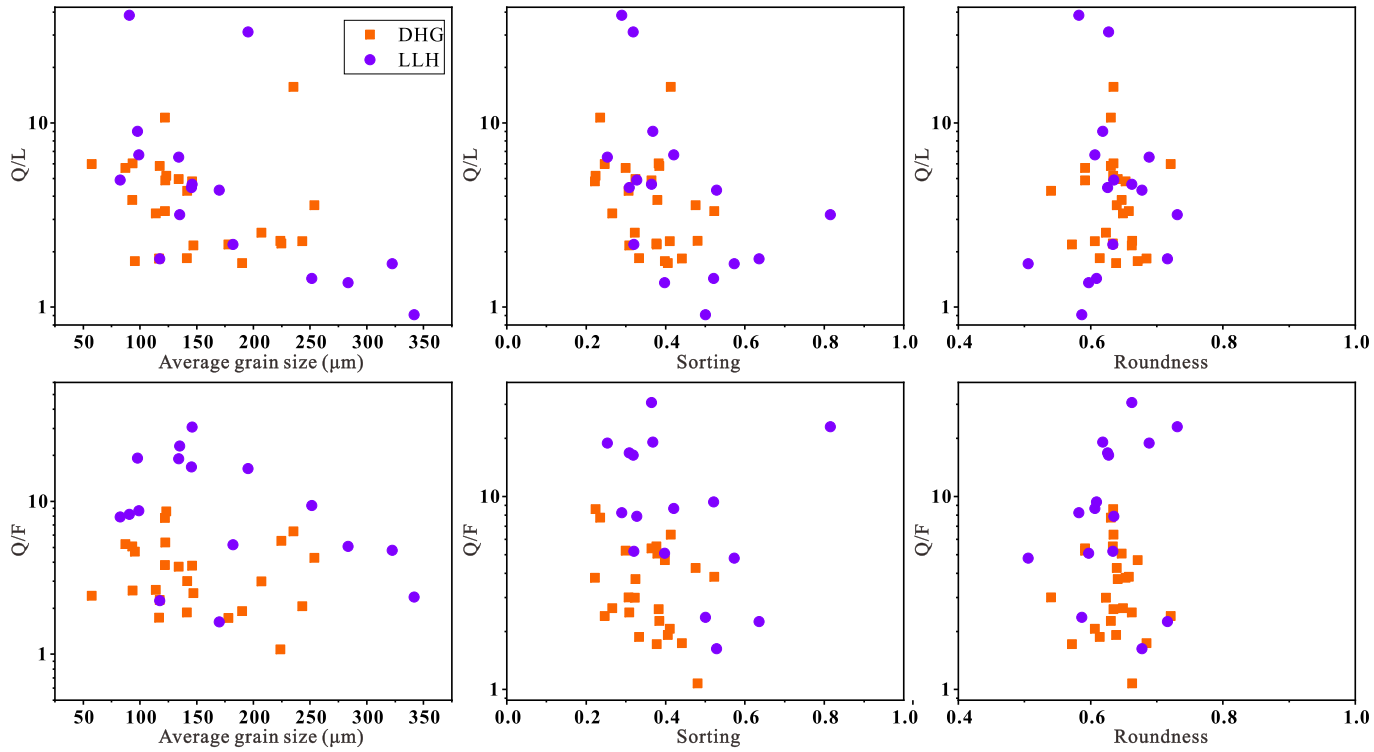

Fig. 13. Relationships between sediment texture (average grain size, sorting, roundness) with sediment composition (quartz/feldspar and quartz/lithic ratios). Note that quartz/lithic ratio exhibit relatively negative correlations with average grain size and sorting, while others have no significant correlations.

Basin when the sedimentary environment was mainly deltaic and lacustrine and sandstones were laminated in siltstone or mudstone strata (Fig. 2) (Cheng et al., 2021).

5.2.3. *Sedimentary recycling*

Due to the widespread distribution of sedimentary and metasedimentary rocks on the Earth's surface, sedimentary recycling is a common process in sedimentary systems (Blatt, 1967; Thomas, 2011). Recycled sandstones are often compositionally enriched in quartz due to its mechanical and chemical stability, and may also contain abundant siltstone, shale, and calcareous lithic fragments (Garzanti et al., 2013). In the Cenozoic Qaidam Basin, sedimentary recycling is prevalent given the widespread exposure of sedimentary strata in the Qilian Mountains (27 %), the Altun Range (8 %), and the Eastern Kunlun Range (19 %). In addition to influencing petrographic composition, recycling also affects grain texture through enhancing the roundness of detrital grains (Garzanti et al., 2022; Shen et al., 2024). Our roundness quantification results reveal predominantly subrounded and rounded grains in the DHG and LLH section samples (Fig. 12), likely indicating contributions from recycled sedimentary rocks. However, grains roundness exhibits no clear temporal variation (Fig. 12) and shows weak correlations with the petrographic compositions, such as Q/F and Q/L ratios (Fig. 13). Detrital zircon U-Pb geochronology may provide insights into recycling from (meta)sedimentary sources. In the DHG section samples, detrital zircon U-Pb age populations vary in the proportion of Precambrian ages (Jian et al., 2024). Samples with higher proportions of Precambrian zircon ages are assumed to reflect greater contributions from recycled sources. Based on this assumption, samples from the DHG section can be divided into two groups, including one with higher recycling contributions and the other with lower contributions. However, grain roundness of detrital grains between these two groups shows no significant difference (Fig. 10C). Given the challenges in discriminating first-cycled and multi-cycled detritus (Garzanti et al., 2013; Pastore et al., 2021; Finzel et al., 2025), the role of sedimentary recycling in provenance interpretation remains an open question requiring further study.

In addition to the factors discussed above, diagenesis, topographic relief, and transport regime also exert controls on sandstone petrographic composition and texture (Johnsson, 1993; Weltje, 2012; Johnsson et al., 2022). For instance, diagenetic overprints (such as overgrowths of quartz grains, precipitation of calcite cements) are documented in both outcrop samples (e.g., Fig. 6E, P) and borehole samples (He et al., 2019; Gong et al., 2023). Nevertheless, our current dataset lacks the resolution to systematically evaluate these influences. Detailed assessment warrants future investigation.

5.3. *How to define sediment source signals for deep-time sedimentary systems*

How to define detrital signals from sediment source regions remains a significant challenge, particularly for deep-time sedimentary systems (Caracciolo, 2020). In the case of the northeastern Qaidam Basin, current controversy regarding sediment provenance interpretations largely arises from uncertainty over whether the Permian–Triassic detrital zircon signals originate from the Qilian Mountains or the Eastern Kunlun Range (e.g., Bush et al., 2016; Cheng et al., 2017, 2021; Wang et al., 2017; Jian et al., 2024). Given this uncertainty, a comprehensive understanding of sediment source signals is of great importance. This study explores this issue from multiple perspectives, as discussed below.

5.3.1. *Potential source terranes need for careful consideration*

Identifying the sources of ancient sedimentary records is inherently challenging due to the combined influences of tectonic and climatic perturbation (Romans et al., 2016), as well as uncertainties of paleogeography and drainage systems. The erosional engine in the deep-time source-to-sink systems may be currently absence or not well-exposed. Accurately determining potential sources is critical for understanding basin-mountain coupling. For the Cenozoic Qaidam Basin, the Songpan-Ganzi Complex was previously thought to be a source of southwestern Qaidam Basin during the early stage of the Cenozoic based on the detrital zircon U-Pb geochronological data, and a 'Paleo-Qaidam Basin'

model during the 50–35 Ma was proposed (McRivette et al., 2019). However, petrographic data suggest that contributions from distal marine sedimentary strata in the Songpan-Ganzi Complex to the southwestern Qaidam Basin can likely be excluded. Sandstones from the Xia Ganchaigou Formation in the southwestern Qaidam Basin have an average modal composition of $Q_{67}F_{20}L_{12}$ (Fig. 8B), in which metamorphic lithics and carbonate lithics are dominating lithic types with a notable absence of sedimentary lithics. These petrographic compositions suggest provenance from granitic plutons, metamorphic rock, and carbonate rocks. Additionally, the sandstones are characterized by subangular to subrounded (Rieser et al., 2005). Coupled compositional and textural immaturity may reveal local and proximal sources from the Eastern Kunlun Range (or Qimantagh region) rather the distal Songpan-Ganzi Complex. Furthermore, Paleoproterozoic zircons, which are prominent in the Songpan-Ganzi Complex, are rarely observed in southwestern Qaidam Basin sandstones (Jian et al., 2024), further supporting our interpretation. Therefore, for the deep-time provenance analysis, the integration of multiple analytical approaches is essential for more accurate reconstructions of source region evolution (Caracciolo, 2020).

5.3.2. *Source signals of a large terrane should not be simply treated as a whole*

The Qilian Mountains represent a large and complex terrane, consisting of four tectonic units. When considering the Qilian Mountains as a single source terrane, late Paleozoic–Mesozoic plutons account for only 2.3 % of the current Qilian Mountains, substantially less than the early Paleozoic plutons (16.5 %; Fig. 1). As a result, the detrital U-Pb age signals from the Qilian Mountains are often characterized by a dominant 410–510 Ma age cluster with neglected Permian–Triassic and Precambrian age populations (e.g., Bush et al., 2016; Wang et al., 2017). However, late Paleozoic–Mesozoic plutons constitute 16.8 % of the North Qaidam terrane (Fig. 1), which serves as a critical sediment source for the northern and northeastern margins of the Qaidam Basin. The dominance of Permian–Triassic age modes in the northern and northeastern Qaidam Basin sandstones could thus be interpreted to be attributed to the North Qaidam terrane rather than the Eastern Kunlun Range (e.g., Cheng et al., 2017; Jian et al., 2024). In petrographic analysis, detailed characterization of individual source terranes could be helpful to understand both local variability and temporal trends in sandstone composition. For example, the high proportion of granitic plutons in the western flank of North Qaidam terrane likely explains the elevated Q/F ratios of samples from the northern Qaidam Basin than those from the northeastern basin (Figs. 1, 10). Temporal changes in sandstone composition, which is related to varied contributions from distinct parent-rock types, could provide insights into discussing the change of provenance and exhumation history of different tectonic domains within the Qilian Mountains. We therefore propose that sedimentary signals from a large, complex source terrane comprising several tectonic belts should not be simply treated as a whole neglecting some important signals (e.g., Wang et al., 2023b). Furthermore, detailed description of source terranes will promote accurate sedimentary provenance studies (e.g., Resentini et al., 2017; Garzanti et al., 2021).

5.3.3. *Heterogeneity of erodibility of different rock types needs attention*

The erodibility of different rocks varies significantly, such as higher erodibility for fragile mudstone or siltstone but lower erodibility for plutons and high-grade metamorphic rocks (Garzanti et al., 2007; Capaldi et al., 2017; Spencer et al., 2018). Such lithological heterogeneity in the potential source terranes leads to differences in sediment yield, which can be reflected in sediment composition and other provenance proxies. The Qilian Mountains, dominated by erodible metamorphic rocks and sedimentary rocks, likely deliver greater sediment volumes than the Eastern Kunlun Range, where resistant plutonic rocks

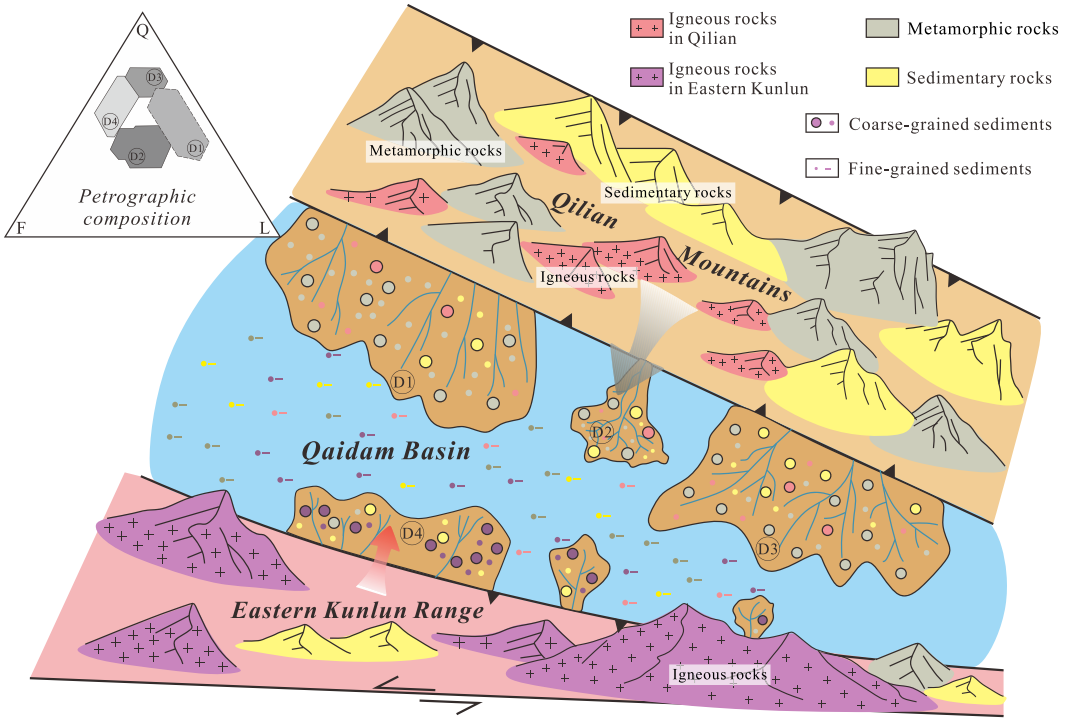

Fig. 14. Schematic model show source-to-sink system of the Cenozoic Qaidam Basin. Coarse-grained sediments (sand, gravel) in the Qaidam Basin are mainly derived from proximal source regions. The Qilian Mountains which are dominated by metamorphic rocks with subordinate sedimentary and igneous rocks largely contribute coarse sediments to the northern and northeastern Qaidam Basin. Contributions from the Eastern Kunlun Range are relatively small and mainly deposited in the south margin of Qaidam Basin. Varied contributions from different rock types in the Qilian Mountains could cause the variation of sandstone petrographic compositions. In contrast, fine-grained sediments (mud, dissolved fraction) from different source regions are well-mixed due to the existence of paleo-megalake (Wang et al., 2023a).

prevail (Fig. 14). This contrast is evidenced by the extensive distribution of alluvial and fluvial coarse sediments along the southern margin of the Qilian Mountains (Zhuang et al., 2011), compared with the relatively thin sedimentary strata along the southern basin margin adjacent to the Eastern Kunlun Range (Fig. 14) (Yin et al., 2008b). Our petrographic data further indicate that samples from regions relatively distant from the Qilian Mountains (e.g., EBL, NBX, YH regions) exhibit high contents of metamorphic lithics and low Q/L ratios (Figs. 8, 11), highlighting the widespread influence of the Qilian Mountains. In addition to tectonics and climate, the lithology-induced differences in sediment flux between the Qilian Mountains and the Eastern Kunlun Range may be the reason for higher sedimentation thickness in the northern Qaidam Basin than the southern basin during the Miocene when both two source terranes were experiencing intense exhumation (Zhuang et al., 2011; Mao et al., 2014; Song et al., 2014; Bao et al., 2017). The modern sedimentary system of the Taiwan Strait offers a useful analogue of the Cenozoic Qaidam Basin. The Taiwan Strait is surrounded by igneous rocks-dominated southeastern China mainland and the (meta)sedimentary rocks-dominated Taiwan Island (Shen et al., 2021). The sediment yield of rivers draining the southeastern China mainland is an order magnitude lower than that of Taiwanese rivers (Milliman and Farnsworth, 2011). As a result, signals from the Taiwanese rivers are widely found in the Taiwan Strait sediments (Horng and Huh, 2011; Shen et al., 2021; Shan et al., 2023). Therefore, we emphasize the importance of considering disproportionate sediment contributions from source terranes with contrasting lithologies in provenance interpretations.

5.4. *Implications for Cenozoic deformation history of the Tibetan Plateau*

The deformation mechanisms of the Tibetan Plateau remain highly debated (Molnar et al., 1993; Tapponnier et al., 2001; Clark, 2012; Ding et al., 2022, and references therein). The growth history of the northern Tibet, which is a far-field response to the India-Eurasia collision, provides critical constraints for evaluating different deformation models of the plateau (Cheng et al., 2021; Jian et al., 2023). Proposed mechanisms for crustal thickening in the northern Tibet include gradual northward propagating shortening model (Tapponnier et al., 2001; Wang et al., 2008; Wang et al., 2017), and synchronous distributed crustal shortening soon after the collision (Jolivet et al., 2001; Clark et al., 2010; Clark, 2012). From the perspective of sedimentary provenance, our petrographic data in the whole Cenozoic Qaidam basin suggests that the northern and northeastern basin were continuously fed by the Qilian Mountains from the Lulehe to the Qigequan formations. In addition, matrix-supported and poor-sorted sandstones in the Lulehe Formation favors high-relief sedimentary environments and localized deposition. As mentioned above, the age model that Cenozoic sedimentation started in the eastly Eocene is preferred in this study. In this case, petrographic analyses indicate that the formation of the Qaidam Basin can be considered as a rapid response to the India-Eurasia collision and further provide evidence for synchronous deformation model of the northern Tibet Plateau.

6. Conclusions and perspectives

An integrated dataset of petrographic composition and grain texture from Cenozoic sandstones in the Qaidam Basin (including new data and previously published data), along with sands in modern rivers draining the Qilian Mountains, allows for a better understanding of the Cenozoic Qaidam Basin sediment source-to-sink system. We contend that the sandstones in the northern and northeastern Qaidam Basin were mainly contributed from the adjacent Qilian Mountains contrasting the opinion that the Eastern Kunlun Range contributed detritus to the northeastern Qaidam Basin based on detrital zircon geochronology. The Altun and Eastern Kunlun ranges are the major sources for sandstones in the western Qaidam Basin. Varied contributions from different parent-rock types in the Qilian Mountains are the reason for the temporal changing of sandstone compositions in the northern and northeastern Qaidam Basin, rather than the source shift from the Eastern Kunlun Range to the Qilian Mountains. Climate and sedimentary environment serve as secondary controls on the sandstone petrographic composition and texture. In addition to tectonic and climate, differences in erodibility among parent-rock types likely contributed to the disproportionate sediment fluxes between the Qilian Mountains and the Eastern Kunlun Range. Provenance analysis based on petrographic data infers that the Qaidam Basin formed as a rapid response to the India-Eurasia collision. This finding further supports the synchronous deformation model of the northern Tibet Plateau.

This study highlights the critical role of sandstone petrography in sedimentary provenance analysis. However, we noticed that sandstone petrography is often ignored or is of secondary importance in many provenance studies. For instance, petrographic data are lacking for small basins in the northeastern Tibetan Plateau (e.g., Subei, Suganhu, and Chaka basins, where detrital zircon geochronology data are available). This gap hampers a more comprehensive understanding of evolution history of the northern Tibetan Plateau from the sandstone petrography perspective. In addition, detailed and proper petrographic analysis of sandstones or sands are helpful for quantitative analysis of source-to-sink system (e.g., Critelli and Ingersoll, 1995; Garzanti and Vezzoli, 2003; Caracciolo et al., 2012b; Resentini et al., 2017; Garzanti, 2019). For example, a detailed classification of metamorphic lithics is fruitful in provenance analysis of foreland-basin sediments shed from Alpine-type collision orogens (Garzanti and Vezzoli, 2003), arc-continent collision in Taiwan (Dorsey, 1988; Garzanti and Resentini, 2016; Resentini et al., 2017). The proper classification of volcanic lithics is proven to provide information on the long-term evolution of volcanic arcs (Critelli and Ingersoll, 1995). Moreover, quantifying sandstone texture, unraveling controlling factors of sandstone petrographic composition and texture, and global-scale sandstone (and modern sand) petrographic big data analyses (e.g., Johnson et al., 2022; Liang et al., 2023; Dong et al., 2024), are important attempts in the field of sediment provenance analysis.

CRediT authorship contribution statement

Xiaotian Shen: Writing – review & editing, Writing – original draft, Visualization, Methodology, Formal analysis, Data curation, Conceptualization. **Xing Jian:** Writing – review & editing, Supervision, Methodology, Investigation, Funding acquisition, Conceptualization. **Wei Zhang:** Writing – review & editing, Resources, Investigation, Funding acquisition. **Shuhuai Ye:** Writing – review & editing, Visualization, Methodology, Formal analysis. **Hanghai Liang:** Writing – review & editing, Methodology, Investigation, Formal analysis. **Yulu Zhuang:** Writing – review & editing, Visualization, Methodology, Formal analysis. **Ping Guan:** Writing – review & editing, Investigation, Funding acquisition.

Declaration of competing interest

The authors declare that they have no known competing financial interests or personal relationships that could have appeared to influence the work reported in this paper.

Acknowledgement

This study was funded by the National Natural Science Foundation of China (Nos. 42476051, 41806052), the Natural Science Foundation of Xiamen, China (No. 3502Z20227006), and the Xiamen University Fundamental Research Funds for the Central Universities (No. 20720160114). We thank Huan Cui, Ruijuan Liu, Fan Feng, Yiqiu Jin, and Ling Fu for their help with sampling. We also appreciate the support from the PetroChina Qinghai Oilfield Company during borehole sample collection. We greatly appreciate the constructive suggestions and

comments from Editor-in-Chief Howard Falcon-Lang and two anonymous reviewers.

Appendix A. Supplementary data

Supplementary data to this article can be found online at https://doi.org/10.1016/j.palaeo.2025.113120.

Data availability

The authors confirm that all data necessary for supporting the scientific findings of this paper have been provided.

References

Bao, J., Wang, Y., Song, C., Feng, Y., Hu, C., Zhong, S., Yang, J., 2017. Cenozoic sediment flux in the Qaidam Basin, northern Tibetan Plateau, and implications with regional tectonics and climate. Glob. Planet. Chang. 155, 56–69. https://doi.org/10.1016/j.gloplacha.2017.03.006.

Bao, J., Song, C., Yang, Y., Fang, X., Meng, Q., Feng, Y., He, P., 2019. Reduced chemical weathering intensity in the Qaidam Basin (NE Tibetan Plateau) during the Late Cenozoic. J. Asian Earth Sci. 170, 155–165. https://doi.org/10.1016/j.jseaes.2018.10.018.

Blatt, H., 1967. Provenance determinations and recycling of sediments. J. Sediment. Petrol. 37, 1031–1044.

Bovet, P.M., Ritts, B.D., Gehrels, G., Abbink, A.O., Darby, B., Hourigan, J., 2009. Evidence of Miocene crustal shortening in the north Qilian Shan from Cenozoic stratigraphy of the western Hexi Corridor, Gansu Province, China. Am. J. Sci. 309 (4), 290–329. https://doi.org/10.2475/00.4009.02.

Bush, M.A., Saylor, J.E., Horton, B.K., Nie, J., 2016. Growth of the Qaidam Basin during Cenozoic exhumation in the northern Tibetan Plateau: Inferences from depositional patterns and multiproxy detrital provenance signatures. Lithosphere 8 (1), 58–82. https://doi.org/10.1130/L449.1.

Capaldi, T.N., Horton, B.K., McKenzie, N.R., Stockli, D.F., Odlum, M.L., 2017. Sediment provenance in contractional orogens: the detrital zircon record from modern rivers in the Andean fold-thrust belt and foreland basin of western Argentina. Earth Planet. Sci. Lett. 479, 83–97. https://doi.org/10.1016/j.epsl.2017.09.001.

Caracciolo, L., 2020. Sediment generation and sediment routing systems from a quantitative provenance analysis perspective: review, application and future development. Earth Sci. Rev. 209, 103226. https://doi.org/10.1016/j.earscirev.2020.103226.

Caracciolo, L., Tolosana-Delgado, R., Le Pera, E., von Eynatten, H., Arribas, J., Tarquini, S., 2012a. Influence of granitoid textural parameters on sediment composition: Implications for sediment generation. Sediment. Geol. 280, 93–107. https://doi.org/10.1016/j.sedgeo.2012.07.005.

Caracciolo, L., Von Eynatten, H., Tolosana-Delgado, R., Critelli, S., Manetti, P., Marchev, P., 2012b. Petrological, geochemical, and statistical analysis of Eocene-Oligocene Sandstones of the Western Thrace Basin, Greece and Bulgaria. J. Sediment. Res. 82 (7), 482–498. https://doi.org/10.2110/jsr.2012.31.

Chen, B., Wang, F., Shi, J., Chen, F., Shi, H., 2019. Origin and sources of minerals and their impact on the hydrocarbon reservoir quality of the Paleogenelulehe Formation in the Eboliang area, northern Qaidam Basin, China. Minerals 9 (7), 436. https://doi.org/10.3390/min9070436.

Cheng, F., Fu, S., Jolivet, M., Zhang, C., Guo, Z., 2016a. Source to sink relation between the Eastern Kunlun Range and the Qaidam Basin, northern Tibetan Plateau, during the Cenozoic. GSA Bull. 128 (1–2), 258–283. https://doi.org/10.1130/B31260.1.

Cheng, F., Jolivet, M., Fu, S., Zhang, C., Zhang, Q., Guom, Z., 2016b. Large-scale displacement along the Altyn Tagh Fault (North Tibet) since its Eocene initiation: insight from detrital zircon U–Pb geochronology and subsurface data. Tectonophysics 677, 261–279. https://doi.org/10.1016/j.tecto.2016.04.023.

Cheng, F., Jolivet, M., Hallot, E., Zhang, D., Zhang, C., Guo, Z., 2017. Tectono-magmatic rejuvenation of the Qaidam craton, northern Tibet. Gondwana Res. 49, 248–263. https://doi.org/10.1016/j.gr.2017.06.004.

Cheng, F., Garzione, C., Jolivet, M., Guo, Z., Zhang, D., Zhang, C., Zhang, Q., 2019a. Initial deformation of the northern Tibetan Plateau: insights from deposition of the Lulehe formation in the Qaidam basin. Tectonics 38, 741–766. https://doi.org/10.1029/2018TC005214.

Cheng, F., Garzione, C.N., Mitra, G., Jolivet, M., Guo, Z., Lu, H., Li, X., Zhang, B., Zhang, C., Zhang, H., Wang, L., 2019b. The interplay between climate and tectonics during the upward and outward growth of the Qilian Shan orogenic wedge, northern Tibetan Plateau. Earth Sci. Rev. 198, 102945. https://doi.org/10.1016/j.earscirev.2019.102945.

Cheng, F., Jolivet, M., Guo, Z., Wang, L., Zhang, C., Li, X., 2021. Cenozoic evolution of the Qaidam basin and implications for the growth of the northern Tibetan plateau: a review. Earth Sci. Rev. 220, 103730. https://doi.org/10.1016/j.earscirev.2021.103730.

Chew, D., O'Sullivan, G., Caracciolo, L., Mark, C., Tyrrell, S., 2020. Sourcing the sand: accessory mineral fertility, analytical and other biases in detrital U–Pb provenance analysis. Earth Sci. Rev. 202, 103093. https://doi.org/10.1016/j.earscirev.2020.103093.

Clark, M.K., 2012. Continental collision slowing due to viscous mantle lithosphere rather than topography. Nature 483 (7387), 74–77. https://doi.org/10.1038/nature10848.

Clark, M., Farley, K., Zheng, D., Wang, Z., Duvall, A., 2010. Early Cenozoic faulting of the northern Tibetan Plateau margin from apatite (U–Th)/He ages. Earth Planet. Sci. Lett. 296 (1), 78–88.

Critelli, S., Ingersoll, R.V., 1995. Neogene synvolcanic deep-marine sandstone of the Topanga Group, Southern California: implications for neovolcanic versus paleovolcanic particles interpretation. Sedimentology 42, 783–804.

Dickinson, W.R., 1985. Interpreting provenance relations from detrital modes of sandstones. In: Zuffa, G.G. (Ed.), Provenance of Arenites, pp. 333–361.

Dickinson, W.R., Suczek, C.A., 1979. Plate tectonics and sandstone compositions. Am. Assoc. Pet. Geol. Bull. 63 (12), 2164–2182. https://doi.org/10.1306/2F9188FB16CE-11D7-8645000102C1865D.

Ding, L., Kapp, P., Cai, F., Garzione, C.N., Xiong, Z., Wang, H., Wang, C., 2022. Timing and mechanisms of Tibetan Plateau uplift. Nat. Rev. Earth Environ. 3 (10), 652–667.

Dong, X., Hu, X., Lai, W., Xue, W., Zhang, S., Zhang, Y., An, W., Fan, H., Chen, S., Li, C., Wang, X., Wu, Y., Chen, L., Zhang, Y., Yu, K., 2024. A global dataset of sandstone detrital composition by Gazzi-Dickinson method. Geosci. Data J. 11, 128–136. https://doi.org/10.1002/gdj3.212.

Dorsey, R.J., 1988. Provenance evolution and unroofing history of a modern arc–continent collision: evidence from petrography of Plio–Pleistocene sandstones, eastern Taiwan. J. Sediment. Petrol. 58, 208–218.

Finzel, E.S., Thomson, S.N., Pearson, D.M., Horkley, L.K., Garber, K., Gardner, C., 2025. First cycle or polycyclic? Combining apatite and zircon detrital U-Pb geochronology and geochemistry to assess sediment recycling and effects of weathering. Earth Planet. Sci. Lett. 650, 119131. https://doi.org/10.1016/j.epsl.2024.119131.

Folk, R.L., 1980. Petrology of Sedimentary Rocks. Austin. Hemphill Publishing Co, USA, p. 182.

Fu, H., Jian, X., Liang, H., Zhang, W., Shen, X., Wang, L., 2022. Tectonic and climatic forcing of chemical weathering intensity in the northeastern Tibetan Plateau since the middle Miocene. Catena 208, 105785. https://doi.org/10.1016/j.catena.2021.105785.

Garzanti, E., 2019. Petrographic classification of sand and sandstone. Earth Sci. Rev. 192, 545–563. https://doi.org/10.1016/j.earscirev.2018.12.014.

Garzanti, E., Andò, S., 2019. Heavy minerals for junior woodchucks. Minerals 9 (3), 148. https://doi.org/10.3390/min9030148.

Garzanti, E., Resentini, A., 2016. Provenance control on chemical indices of weathering (Taiwan river sands). Sediment. Geol. 336, 81–95. https://doi.org/10.1016/j.sedgeo.2015.06.013.

Garzanti, E., Vezzoli, G., 2003. A classification of metamorphic grains in sands based on their composition and grade. J. Sediment. Res. 73 (5), 830–837.

Garzanti, E., Doglioni, C., Vezzoli, G., Andò, S., 2007. Orogenic belts and orogenic sediment provenance. J. Geol. 115 (3), 315–334.

Garzanti, E., Andò, S., Vezzoli, G., 2008. Settling equivalence of detrital minerals and grainsize dependence of sediment composition. Earth Planet. Sci. Lett. 273 (1–2), 138–151. https://doi.org/10.1016/j.epsl.2008.06.020.

Garzanti, E., Andò, S., Vezzoli, G., 2009. Grain-size dependence of sediment composition and environmental bias in provenance studies. Earth Planet. Sci. Lett. 277 (3–4), 422–432. https://doi.org/10.1016/j.epsl.2008.11.007.

Garzanti, E., Limonta, M., Resentini, A., Bandopadhyay, P.C., Najman, Y., Andò, S., Vezzoli, G., 2013. Sediment recycling at convergent plate margins (Indo-Burman ranges and Andaman–Nicobar Ridge). Earth Sci. Rev. 123, 113–132. https://doi.org/10.1016/j.earscirev.2013.04.008.

Garzanti, E., He, J., Barbarano, M., Resentini, A., Li, C., Yang, L., Yang, S., Wang, H., 2021. Provenance versus weathering control on sediment composition in tropical monsoonal climate (South China)-2. Sand petrology and heavy minerals. Chem. Geol. 564, 119997. https://doi.org/10.1016/j.chemgeo.2020.119997.

Garzanti, E., Pastore, G., Stone, A., Vainer, S., Vermeesch, P., Resentini, A., 2022. Provenance of Kalahari Sand: paleoweathering and recycling in a linked fluvial-aeolian system. Earth Sci. Rev. 224, 103867. https://doi.org/10.1016/j.earscirev.2021.103867.

Gehrels, G.E., Yin, A., Wang, X.F., 2003. Magmatic history of the northeastern Tibetan Plateau. J. Geophys. Res. Solid Earth 108 (B9). https://doi.org/10.1029/2002JB001876.

Gong, L., Gao, X., Qu, F., Zhang, Y., Zhang, G., Zhu, J., 2023. Reservoir quality and controlling mechanism of the Upper Paleogene Fine-Grained Sandstones in Lacustrine Basin in the Hinterlands of Northern Qaidam Basin, NW China. J. Earth Sci. 34 (3), 806–823. https://doi.org/10.1007/s12583-022-1701-6.

Guan, P., Jian, X., 2013. The Cenozoic sedimentary record in Qaidam basin and its implications for tectonic evolution of the northern Tibetan plateau (in Chinese with English Abstract). Acta Sedimentol. Sin. 31, 824–833. https://doi.org/10.14027/j.cnki.cjxb.2013.05.014.

Guo, P., Liu, C., Huang, L., Wang, P., Wang, K., Yuan, H., Xu, C., Zhang, Y., 2017. Genesis of the late Eocene bedded halite in the Qaidam Basin and its implication for paleoclimate in East Asia. Palaeogeogr. Palaeoclimatol. Palaeoecol. 487, 364–380. https://doi.org/10.1016/j.palaeo.2017.09.023.

He, J., Wang, H., Zhang, C., Yang, X., Shangguan, Y., Zhao, R., Gong, Y., Wu, Z., 2019. A comprehensive analysis of the sedimentology, petrography, diagenesis and reservoir quality of sandstones from the Oligocene Xiaganchaigou (E_3) Formation in the Lengdong area, Qaidam Basin, China. J. Pet. Explor. Prod. Technol. 9, 953–969. https://doi.org/10.1007/s13202-018-0571-z.

He, P., Song, C., Wang, Y., Wang, D., Chen, L., Meng, Q., Fang, X., 2021. Early Cenozoic activated deformation in the Qilian Shan, northeastern Tibetan Plateau: Insights from detrital apatite fission-track analysis. Basin Res. 33 (3), 1731–1748. https://doi.org/10.1111/bre.12533.

Hong, D., Jian, X., Fu, L., Zhang, W., 2020. Garnet trace element geochemistry as a sediment provenance indicator: an example from the Qaidam basin, northern Tibet. Mar. Pet. Geol. 116, 104316. https://doi.org/10.1016/j.marpetgeo.2020.104316.

Horng, C.S., Huh, C.-A., 2011. Magnetic properties as tracers for source-to-sink dispersal of sediments: a case study in the Taiwan Strait. Earth Planet. Sci. Lett. 309 (1–2), 141–152. https://doi.org/10.1016/j.epsl.2011.07.002.

Ingersoll, R.V., Bullard, T.F., Ford, R.L., Grimm, J.D., Pickle, J.D., Sares, S.W., 1984. The effect of grain-size on detrital modes: a test of the Gazzi-Dickinson point-counting method. J. Sediment. Petrol. 54 (1), 103–116. https://doi.org/10.1306/212F83B92B24-11D7-8648000102C1865D.

Ji, J., Zhang, K., Clift, P.D., Zhuang, G., Song, B., Ke, X., Xu, Y., 2017. High-resolution magnetostratigraphic study of the Paleogene-Neogene strata in the Northern Qaidam Basin: implications for the growth of the Northeastern Tibetan Plateau. Gondwana Res. 46, 141–155. https://doi.org/10.1016/j.gr.2017.02.015.

Jian, X., Guan, P., Zhang, D.W., Zhang, W., Feng, F., Liu, R.J., Lin, S.D., 2013a. Provenance of Tertiary sandstone in the northern Qaidam basin, northeastern Tibetan Plateau: integration of framework petrography, heavy mineral analysis and mineral chemistry. Sediment. Geol. 290, 109–125. https://doi.org/10.1016/j.sedgeo.2013.03.010.

Jian, X., Guan, P., Zhang, W., Feng, F., 2013b. Geochemistry of Mesozoic and Cenozoic sediments in the northern Qaidam basin, northeastern Tibetan Plateau: implications for provenance and weathering. Chem. Geol. 360, 74–88. https://doi.org/10.1016/j.chemgeo.2013.10.011.

Jian, X., Guan, P., Fu, S.-T., Zhang, D.-W., Zhang, W., Zhang, Y.-S., 2014. Miocene sedimentary environment and climate change in the northwestern Qaidam basin, northeastern Tibetan Plateau: Facies, biomarker and stable isotopic evidences. Palaeogeogr. Palaeoclimatol. Palaeoecol. 414, 320–331. https://doi.org/10.1016/j.palaeo.2014.09.011.

Jian, X., Guan, P., Zhang, W., Liang, H., Feng, F., Fu, L., 2018. Late cretaceous to early Eocene deformation in the northern Tibetan Plateau: detrital apatite fission track evidence from northern Qaidam basin. Gondwana Res. 60, 94–104. https://doi.org/10.1016/j.gr.2018.04.007.

Jian, X., Weislogel, A., Pullen, A., Shang, F., 2020. Formation and evolution of the Eastern Kunlun Range, northern Tibet: evidence from detrital zircon U-Pb geochronology and Hf isotopes. Gondwana Res. 83, 63–79. https://doi.org/10.1016/j.gr.2020.01.015.

Jian, X., Fu, L., Wang, P., Guan, P., Zhang, W., Fu, H., Mei, H., 2023. Sediment provenance of the Lulehe Formation in the Qaidam basin: Insight to initial Cenozoic deposition and deformation in northern Tibetan plateau. Basin Res. 35 (1), 271–294. https://doi.org/10.1111/bre.12712.

Jian, X., Guan, P., Fu, L., Zhang, W., Shen, X., Fu, H., Wang, L., 2024. Detrital zircon geochronology and provenance of Cenozoic deposits in the Qaidam basin, northern Tibetan plateau: an overview with new data, implications and perspectives. Mar. Pet. Geol. 159, 106566. https://doi.org/10.1016/j.marpetgeo.2023.106566.

Johnson, J.I., Sharman, G.R., Szymanski, E., Huang, X., 2022. Machine learning applied to a modern-Pleistocene petrographic data set: the global prediction of sand modal composition (GloPrSM) model. J. Geophys. Res. Earth 127 (7), e2022JF006595. https://doi.org/10.1029/2022JF006595.

Johnsson, M.J., 1993. The system controlling the composition of clastic sediments. In: Johnsson, M.J., Basu, A. (Eds.), Processes Controlling the Composition of Clastic Sediments, 284. Geological Society of America, Special Papervol, pp. 1–19.

Jolivet, M., Brunel, M., Seward, D., Xu, Z., Yang, J., Roger, F., Tapponnier, P., Malavieille, J., Arnaud, N., Wu, C., 2001. Mesozoic and Cenozoic tectonics of the northern edge of the Tibetan plateau: fission-track constraints. Tectonophysics 343 (1–2), 111–134. https://doi.org/10.1016/S0040-1951(01)00196-2.

Lawrence, R.L., Cox, R., Mapes, R.W., Coleman, D.S., 2011. Hydrodynamic fractionation of zircon age populations. Geol. Soc. Am. Bull. 123 (1–2), 295–305. https://doi.org/10.1130/b30151.1.

Li, W., Neubauer, F., Liu, Y., Genser, J., Ren, S., Han, G., Liang, C., 2013. Paleozoic evolution of the Qimantagh magmatic arcs, Eastern Kunlun Mountains: Constraints from zircon dating of granitoids and modern river sands. J. Asian Earth Sci. 77, 183–202. https://doi.org/10.1016/j.jseaes.2013.08.030.

Li, L., Wu, C., Yu, X., 2018. Cenozoic evolution of the Altyn Tagh and East Kunlun fault zones inferred from detrital garnet, tourmaline and rutile in southwestern Qaidam Basin (Northern Tibetan Plateau). Basin Res. 30 (1), 35–58. https://doi.org/10.1111/bre.12241.

Li, B., Zuza, A.V., Chen, X., Hu, D., Shao, Z., Qi, B., Wang, Z., Levy, D.A., Xiong, X., 2020. Cenozoic multi-phase deformation in the Qilian Shan and out-of-sequence development of the northern Tibetan Plateau. Tectonophysics 782, 228423. https://doi.org/10.1016/j.tecto.2020.228423.

Li, C., Zheng, D., Zhou, R., Wang, W., Yu, J., Liu, C., Wang, Y., Pang, J., Ma, Y., Hao, Y., Li, Y., Wang, X., 2021. Topographic growth of the northeastern Tibetan Plateau during the middle-late Miocene: insights from integrated provenance analysis in the NE Qaidam Basin. Basin Res. 33 (6), 3212–3230. https://doi.org/10.1111/bre.12600.

Li, B., Wang, Y., Zuza, A.V., Chen, X., Shao, Z., Wang, Z.-Z., Sun, Y., Wu, C., 2023. Cenozoic deformation in the eastern domain of the North Qaidam thrust belt, northern Tibetan Plateau. GSA Bull. 135 (1–2), 331–350. https://doi.org/10.1130/B36215.1.

Liang, Y., Zhang, B., Zhang, Y., Zhang, Y., Wang, J., Liu, Z., 2021. Evolution of the Miocene megalake in the western Qaidam Basin, northwestern China. Palaeogeogr. Palaeoclimatol. Palaeoecol. 571, 110384. https://doi.org/10.1016/j.palaeo.2021.110384.

Liang, W., Hu, X., Garzanti, E., Wen, H., Hou, M., 2023. Petrographic composition and heavy minerals in modern river sand: a global database. Geosci. Data J. 00, 1–9. https://doi.org/10.1002/gdj3.219.

Liu, D., Fang, X., Wang, Y., Zhang, W., Gao, J., 2008. Cenozoic deformation history determined by restoration of the balanced section across the Qaidam Basin. Chin. J. Geol. 43 (4), 637–647 (in Chinese with English abstract).

Liu, Y., Yang, Y., Song, B., Galy, A., Zhang, F., Jin, Z., Zhang, G., Ye, C., Fang, X., 2022. Hydrothermal systems with radiogenic Sr in the North Qaidam ultrahigh-pressure metamorphic belt, NE Tibetan Plateau and implications for regional dissolved Sr budge. Appl. Geochem. 138, 105214. https://doi.org/10.1016/j.apgeochem.2022.105214.

Liu, Y., Yang, Y., Yang, R., Galy, A., Jin, Z., Fang, X., Song, B., 2023. Deciphering source-to-sink history from a solute perspective: a Sr isotope approach in the Qaidam Basin, NE Tibet. Gondwana Res. 118, 76–91. https://doi.org/10.1016/j.gr.2023.02.012.

Lu, H., Ye, J., Guo, L., Pan, J., Xiong, S., Li, H., 2019. Towards a clarification of the provenance of Cenozoic sediments in the northern Qaidam Basin. Lithosphere 11 (2), 252–272. https://doi.org/10.1130/L1037.1.

Lu, H., Sang, S., Wang, P., Zhang, Z., Pan, J., Li, H., 2022. Initial uplift of the Qilian Shan, northern Tibet since ca. 25 Ma: Implications for regional tectonics and origin of eolian deposition in Asia. GSA Bull. 134 (9–10), 2531–2547. https://doi.org/10.1130/B36242.1.

Malusà, M.G., Carter, A., Limoncelli, M., Villa, I.M., Garzanti, E., 2013. Bias in detrital zircon geochronology and thermochronometry. Chem. Geol. 359, 90–107. https://doi.org/10.1016/j.chemgeo.2013.09.016.

Malusà, M.G., Resentini, A., Garzanti, E., 2016. Hydraulic sorting and mineral fertility bias in detrital geochronology. Gondwana Res. 31, 1–19. https://doi.org/10.1016/j.gr.2015.09.002.

Mao, L., Xiao, A., Wu, L., Li, B., Wang, L., Lou, Q., Dong, Y., Qin, S., 2014. Cenozoic tectonic and sedimentary evolution of southern Qaidam Basin, NE Tibetan Plateau and its implication for the rejuvenation of Eastern Kunlun Mountains. Sci. China Earth Sci. 57 (11), 2726–2739.

Mattinson, C.G., Menold, C.A., Zhang, J.X., Bird, D.K., 2007. High-and ultrahigh-pressure metamorphism in the North Qaidam and South Altyn terranes, western China. Int. Geol. Rev. 49 (11), 969–995. https://doi.org/10.2747/0020-6814.49.11.969.

McRivette, M.W., Yin, A., Chen, X., Gehrels, G.E., 2019. Cenozoic basin evolution of the central Tibetan plateau as constrained by U-Pb detrital zircon geochronology, sandstone petrology, and fission-track thermochronology. Tectonophysics 751, 150–179. https://doi.org/10.1016/j.tecto.2018.12.015.

Miao, Y., Fang, X., Wu, F., Cai, M., Song, C., Meng, Q., Xu, L., 2013. Late Cenozoic continuous aridification in the western Qaidam Basin: evidence from sporopollen records. Clim. Past 9 (4), 1863–1877. https://doi.org/10.5194/cp-9-1863-2013.

Milliman, J.D., Farnsworth, K.L., 2011. Runoff, erosion, and delivery to the Coastal Ocean. In: River Discharge to the Coastal Ocean: A Global Synthesis. Cambridge University Press, pp. 13–69. https://doi.org/10.1017/CBO9780511781247.003.

Molnar, P., England, P., Martinod, J., 1993. Mantle dynamics, uplift of the Tibetan Plateau, and the Indian monsoon. Rev. Geophys. 31 (4), 357–396.

Nie, J., Ren, X., Saylor, J.E., Su, Q., Horton, B.K., Bush, M.A., Chen, W., Pfaff, K., 2020. Magnetic polarity stratigraphy, provenance, and paleoclimate analysis of Cenozoic strata in the Qaidam Basin, NE Tibetan Plateau. GSA Bull. 132 (1–2), 310–320. https://doi.org/10.1130/B35175.1.

Palomares, M., Arribas, J., 1993. Modern stream sands from compound crystalline sources: composition and sand generation index. In: Johnsson, M.J., Basu, A. (Eds.), Processes Controlling the Composition of Clastic Sediments, 284. Geological Society of Ameria Special Paper, pp. 313–322.

Pang, X., Zhao, W., Su, A., Zhang, S., Li, M., Dang, Y., Xu, F., Zhou, R., Zhang, D., Xu, Z., Guan, Z., Chen, J., Li, S., 2005. Geochemistry and origin of the giant Quaternary shallow gas accumulations in the eastern Qaidam Basin, NW China. Org. Geochem. 36, 1636–1649. https://doi.org/10.1016/j.orggeochem.2005.08.013.

Pastore, G., Baird, T., Vermeesch, P., Bristow, C., Resentini, A., Garzanti, E., 2021. Provenance and recycling of Sahara Desert sand. Earth Sci. Rev. 216, 103606. https://doi.org/10.1016/j.earscirev.2021.103606.

Pullen, A., Kapp, P., McCallister, A.T., Chang, H., Gehrels, G.E., Garzione, C.N., Heermance, R.V., Ding, L., 2011. Qaidam Basin and northern Tibetan Plateau as dust sources for the Chinese Loess Plateau and paleoclimatic implications. Geology 39 (11), 1031–1034. https://doi.org/10.1130/G32296.1.

Ren, X., Nie, J., Saylor, J.E., Li, H., Bush, M.A., Horton, B.K., 2019. Provenance control on chemical weathering index of fluvio-lacustrine sediments: evidence from the Qaidam Basin, NE Tibetan plateau. Geochem. Geophys. Geosyst. 20 (7), 3216–3224. https://doi.org/10.1029/2019gc008330.

Resentini, A., Goren, L., Castelltort, S., Garzanti, E., 2017. Partitioning sediment flux by provenance and tracing erosion patterns in Taiwan. J. Geophys. Res. Earth 122 (7), 1430–1454. https://doi.org/10.1002/2016jf004026.

Resentini, A., Andò, S., Garzanti, E., 2018. Quantifying roundness of detrital minerals by image analysis: sediment transport, shape effects, and provenance implications. J. Sediment. Res. 88 (2), 276–289. https://doi.org/10.2110/jsr.2018.12.

Rieser, A.B., Neubauer, F., Liu, Y., Ge, X., 2005. Sandstone provenance of north-western sectors of the intracontinental Cenozoic Qaidam basin, western China: Tectonic vs. climatic control. Sediment. Geol. 177 (1–2), 1–18. https://doi.org/10.1016/j.sedgeo.2005.01.012.

Rieser, A.B., Liu, Y., Genser, J., Neubauer, F., Handler, R., Ge, X.-H., 2006a. Uniform Permian 40Ar/39Ar detrital mica ages in the eastern Qaidam Basin (NW China): where is the source? Terra Nova 18 (1), 79–87. https://doi.org/10.1111/j.1365-3121.2005.00666.x.

Rieser, A.B., Liu, Y., Genser, J., Newbauer, F., Handler, R., Friedl, G., Ge, X.-H., 2006b. 40Ar/39Ar ages of detrital white mica constrain the Cenozoic development of the intracontinental Qaidam Basin, China. Geol. Soc. Am. Bull. 118 (11–12), 1522–1534. https://doi.org/10.1130/B25962.1.

Romans, B.W., Castelltort, S., Covault, J.A., Fildani, A., Walsh, J.P., 2016. Environmental signal propagation in sedimentary systems across timescales. Earth Sci. Rev. 153, 7–29.

Shan, X., Dalrymple, R.W., Shi, X., Jin, L., Liu, S., Liu, C., Liu, S., Qiao, S., Zhou, Q., Fang, X., 2023. Changjiang coastal mud-belt deposits in Taiwan Strait: Controls on

its distribution and facies. Sedimentology 70 (4), 1131–1163. https://doi.org/10.1111/sed.13076.
Shen, X., Jian, X., Li, C., Liu, J.T., Chang, Y.-P., Zhang, S., Mei, H., Fu, H., Zhang, W., 2021. Submarine topography-related spatial variability of the southern Taiwan Strait sands (East Asia). Mar. Geol. 436, 106495. https://doi.org/10.1016/j.margeo.2021.106495.
Shen, X., Jian, X., Zhang, W., Guan, P., 2024. Grain textural bias in detrital single-mineral provenance studies. Sediment. Geol. 471, 106731. https://doi.org/10.1016/j.sedgeo.2024.106731.
Song, S., Niu, Y., Zhang, L., Wei, C., Liou, J.G., Su, L., 2009. Tectonic evolution of early Paleozoic HP metamorphic rocks in the North Qilian Mountains, NW China: new perspectives. J. Asian Earth Sci. 35 (3–4), 334–353. https://doi.org/10.1016/j.jseaes.2008.11.005.
Song, B., Zhang, K., Lu, J., Wang, C., Xu, Y., 2013. The middle Eocene to early Miocene integrated sedimentary record in the Qaidam Basin and its implications for paleoclimate and early Tibetan Plateau uplift. Can. J. Earth Sci. 50 (2), 183–196. https://doi.org/10.1139/cjes-2012-0048.
Song, C., Hu, S., Han, W., Zhang, T., Fang, X., Gao, J., Wu, F., 2014. Middle Miocene to earliest Pliocene sedimentological and geochemical records of climate change in the western Qaidam Basin on the NE Tibetan Plateau. Palaeogeogr. Palaeoclimatol. Palaeoecol. 395, 67–76.
Song, B., Zhang, K., Hou, Y., Ji, J., Wang, J., Yang, Y., Yang, T., Wang, C., Shen, T., 2019. New insights into the provenance of Cenozoic strata in the Qaidam Basin, northern Tibet: Constraints from combined U-Pb dating of detrital zircons in recent and ancient fluvial sediments. Palaeogeogr. Palaeoclimatol. Palaeoecol. 533, 109254. https://doi.org/10.1016/j.palaeo.2019.109254.
Spencer, C.J., Kirkland, C.L., Roberts, N.M.W., 2018. Implications of erosion and bedrock composition on zircon fertility: examples from South America and Western Australia. Terra Nova 30 (4), 289–295. https://doi.org/10.1111/ter.12338.
Sun, Z., Yang, Z., Pei, J., Ge, X., Wang, X., Yang, T., Li, W., Yuan, S., 2005. Magnetostratigraphy of Paleogene sediments from northern Qaidam Basin, China: implications for tectonic uplift and block rotation in northern Tibetan plateau. Earth Planet. Sci. Lett. 237 (3–4), 635–646. https://doi.org/10.1016/j.epsl.2005.07.007.
Sun, Y., Liu, J., Liang, Y., Ji, J., Liu, W., Aitchison, J.C., Sun, J., Lu, J., Song, B., Xu, Y., Zhang, K., Liu, Z., 2020a. Cenozoic moisture fluctuations on the northeastern Tibetan Plateau and association with global climatic conditions. J. Asian Earth Sci. 200, 104490. https://doi.org/10.1016/j.jseaes.2020.104490.
Sun, G., Wang, M., Guo, J., Wang, Y., Yang, Y., 2020b. Geochemical significance of clay minerals and elements in paleogene sandstones in the center of the northern margin of the Qaidam Basin, China. Minerals 10 (6), 505. https://doi.org/10.3390/min10060505.
Tapponnier, P., Xu, Z., Roger, F., Meyer, B., Arnaud, N., Wittlinger, G., Yang, J., 2001. Oblique stepwise rise and growth of the Tibet Plateau. Science 294 (5547), 1671–1677. https://doi.org/10.1126/science.105978.
Thomas, W.A., 2011. Detrital-zircon geochronology and sedimentary provenance. Lithosphere 3 (4), 304–308.
Wadell, H., 1932. Volume, shape and roundness of rock particles. J. Geol. 40, 443–451.
Wang, C., Zhao, X., Liu, Z., Lippert, P.C., Graham, S.A., Coe, R.S., Yi, H., Zhu, L., Liu, S., Li, Y., 2008. Constraints on the early uplift history of the Tibetan plateau. Proc. Natl. Acad. Sci. 105, 4987–4992. https://doi.org/10.1073/pnas.0703595105.
Wang, W., Zheng, W., Zhang, P., Li, Q., Kirby, E., Yuan, D., Zheng, D., Liu, C., Wang, Z., Zhang, H., Pang, J., 2017. Expansion of the Tibetan Plateau during the Neogene. Nat. Commun. 8 (1), 15887. https://doi.org/10.1038/ncomms15887.
Wang, W., Zhang, P., Garzione, C.N., Liu, C., Zhang, Z., Pang, J., Wang, Y., Zheng, D., Zheng, W., Zhang, H., 2022. Pulsed rise and growth of the Tibetan Plateau to its northern margin since ca. 30 Ma. Proc. Natl. Acad. Sci. 119 (8), e2120364119. https://doi.org/10.1073/pnas.2120364119.
Wang, L., Jian, X., Fu, H., Zhang, W., Shang, F., Fu, L., 2023a. Decoupled local climate and chemical weathering intensity of fine-grained siliciclastic sediments from a paleomegalake: an example from the Qaidam basin, northern Tibetan Plateau. Sediment. Geol. 454, 106462. https://doi.org/10.1016/j.sedgeo.2023.106462.
Wang, Y., Sun, G., Bo, S., Fu, S., Cruset, D., Martín-Martín, J.D., Guo, H., Cantarero, I., Baqués, V., Chen, G., Zhang, S., Travé, A., 2023b. Detrital zircon U-Pb dating and geochemistry of the Paleogene-Neogene sediments in the Qaidam Basin (China): Implications for provenance and tectonics. Glob. Planet. Chang. 228, 104202. https://doi.org/10.1016/j.gloplacha.2023.104202.
Weltje, G.J., 2012. Quantitative models of sediment generation and provenance: state of the art and future developments. Sediment. Geol. 280, 4–20. https://doi.org/10.1016/j.sedgeo.2012.03.010.
Weltje, G.J., von Eynatten, H., 2004. Quantitative provenance analysis of sediments: review and outlook. Sediment. Geol. 171 (1–4), 1–11. https://doi.org/10.1016/j.sedgeo.2004.05.007.
Wu, C., Zuza, A.V., Yin, A., Liu, C., Reith, R.C., Zhang, J., Liu, W., Zhou, Z., 2017. Geochronology and geochemistry of Neoproterozoic granitoids in the central Qilian Shan of northern Tibet: Reconstructing the amalgamation processes and tectonic history of Asia. Lithosphere 9 (4), 609–636. https://doi.org/10.1130/L640.1.
Xia, G., Wu, C., Li, G., Li, G., Yi, H., Wagreich, M., 2021. Cenozoic growth of the Eastern Kunlun Range (northern Tibetan Plateau): evidence from sedimentary records in the southwest Qaidam Basin. Int. Geol. Rev. 63 (6), 769–786. https://doi.org/10.1080/00206814.2020.1731717.
Yan, Z., Yang, R., Yang, Y., Liu, Y., Galy, A., Fang, X., 2024. Late Miocene drainage reorganization on the NE Tibetan Plateau linked to growth of the Qilian Shan revealed by coupled carbonate Sr-silicate Nd isotopic tracers. Palaeogeogr. Palaeoclimatol. Palaeoecol. 638, 112038. https://doi.org/10.1016/j.palaeo.2024.112038.
Yang, J., Wu, C., Zhang, J., Shi, R., Meng, F., Wooden, J., Yang, H.-Y., 2006. Protolith of eclogites in the north Qaidam and Altun UHP terrane, NW China: earlier oceanic crust? J. Asian Earth Sci. 28 (2–3), 185–204. https://doi.org/10.1016/j.jseaes.2005.09.020.
Yang, S., Zhang, F., Wang, Z., 2012. Grain size distribution and age population of detrital zircons from the Changjiang (Yangtze) river system, China. Chem. Geol. 296–297, 26–38. https://doi.org/10.1016/j.chemgeo.2011.12.016.
Ye, S., Jian, X., Fu, L., Zhang, W., Shen, X., Guan, P., 2024. Detrital muscovite 40Ar/39Ar geochronology and provenance of Cenozoic deposits in the Qaidam basin, northern Tibetan Plateau and comparison with detrital zircon and apatite records. Mar. Pet. Geol. 169, 107068. https://doi.org/10.1016/j.marpetgeo.2024.107068.
Yin, A., Dang, Y.-Q., Wang, L.-C., Jiang, W.-M., Zhou, S.-P., Chen, X.-H., Gehrels, G.E., McRivette, M.W., 2008a. Cenozoic tectonic evolution of Qaidam basin and its surrounding regions (Part 1): the southern Qilian Shan-Nan Shan thrust belt and northern Qaidam basin. Geol. Soc. Am. Bull. 120 (7–8), 813–846 doi: 10.1130.B26180.1.
Yin, A., Dang, Y.-Q., Zhang, M., Chen, X.H., McRivette, M.W., 2008b. Cenozoic tectonic evolution of the Qaidam basin and its surrounding regions (Part 3): structural geology, sedimentation, and regional tectonic reconstruction. Geol. Soc. Am. Bull. 120 (7–8), 847–876. https://doi.org/10.1130/B26232.1.
Zeng, D., Ding, L., Spicer, R.A., Wang, C., Wu, C., Wang, X., Widdowson, M., Xie, J., Yue, Y., Zhao, C., Guo, X., 2025. Direct dating of Qaidam Basin stratigraphy, Northern Tibet. Earth Planet. Sci. Lett. 664, 119440.
Zhang, W., Jian, X., Fu, L., Feng, F., Guan, P., 2018. Reservoir characterization and hydrocarbon accumulation in late Cenozoic lacustrine mixed carbonate-siliciclastic fine-grained deposits of the northwestern Qaidam basin, NW China. Mar. Pet. Geol. 98, 675–686. https://doi.org/10.1016/j.marpetgeo.2018.09.008.
Zhang, S., Jian, X., Pullen, A., Fu, L., Liang, H., Hong, D., Zhang, W., 2021. Tectono-magmatic events of the Qilian orogenic belt in northern Tibet: new insights from detrital zircon geochronology of river sands. Int. Geol. Rev. 63 (8), 917–940. https://doi.org/10.1080/00206814.2020.1734876.
Zhou, H., Chen, L., Diwu, C., Lei, C., 2018. Cenozoic uplift of the Qimantage Mountains, northeastern Tibet: contraints from provenance analysis of Cenozoic sediments in Qaidam Basin. Geol. J. 53 (6), 2613–2632. https://doi.org/10.1002/gj.3095.
Zhu, W., Wu, C., Wang, J., Zhou, T., Li, J., Zhang, C., Li, L., 2017. Heavy mineral compositions and zircon U-Pb ages of Cenozoic sandstones in the SW Qaidam basin, northern Tibetan Plateau: implications for provenance and tectonic setting. J. Asian Earth Sci. 146, 233–250. https://doi.org/10.1016/j.jseaes.2017.05.023.
Zhuang, G., Hourigan, J.K., Ritts, B.D., Kent-Corson, M.L., 2011. Cenozoic multiple-phase tectonic evolution of the northern Tibetan Plateau: constraints from sedimentary records from Qaidam basin, Hexi Corridor, and Subei basin, Northwest China. Am. J. Sci. 311 (2), 116–152. https://doi.org/10.2475/02.2011.02.
Zuza, A.V., Wu, C., Reith, R.C., Yin, A., Li, J., Zhang, J., Zhang, Y., Wu, L., Liu, W., 2018. Tectonic evolution of the Qilian Shan: an early Paleozoic orogen reactivated in the Cenozoic. GSA Bull. 130 (5–6), 881–925. https://doi.org/10.1130/B31721.1.